

---

## CHAPTER 4: CFD MODELLING AND BASE CASE VERIFICATION

---

The objective of this dissertation is to ultimately perform design optimisation of the SEN using CFD modelling, in order to achieve an optimum SEN in the continuous casting process. This will involve the set-up and solution of multiple CFD models. The first step towards this goal is to model the base case (starting point of the optimisation exercise), which is usually a current SEN design. As soon as confidence in the CFD modelling process is achieved (by the end of this chapter), different SEN designs can be evaluated for optimisation purposes (Chapter 5).

By the end of this chapter, the reader will be convinced that the methods followed to model a typical SEN and mould set-up is reliable and will ensure correct CFD solution flow fields, as these solutions are validated with water model experiments.

### **4.1 Approach: CFD modelling of base case design**

A CFD model of any engineering flow application involves a number of inputs by the user to be physically representative of the real flow situation. These inputs involve a wide range of issues from grid generation (type of grid-elements, and geometric simplifications, *inter alia*) to turbulence modelling (choice of models to use to simulate physical turbulence) [28]. All these choices necessarily alter the simplified forms of the Navier-Stokes equations and will have a large impact on the validity of the solutions of the CFD model.

The CFD modelling of the flow (and heat transfer) in the SEN and mould of the continuous casting process is no different: the author had to make a number of choices, assumptions and geometric adjustments and/or simplifications that can have (and had) an impact on the ultimate solution.

Modelling the base case SEN and mould in the continuous casting process using CFD techniques, involves some trial and error work and a survey of the available literature<sup>1</sup> to determine which options in the CFD code suit the flow situation in question best. Obtaining a solution for the base case that is not only physical correct, but also robust, is crucial for a design optimisation exercise.

The approach followed to develop a robust method (from geometry and mesh generation to modelling options and assumptions) for this dissertation, is briefly described in the sections to follow.

#### **4.1.1 General approach to modelling the base case**

As already stated in the previous chapters, when confronted with the problem to model the SEN and mould with CFD techniques, the obvious first step is the generation of the physical geometry. The next step is to divide the geometry in elements or volumes (meshing the geometry). Thereafter, the boundaries of the geometry must be defined in the pre-processor (GAMBIT [11] in this dissertation) to be recognised by the CFD code (FLUENT [10] in this dissertation).

After importing the geometry and mesh into FLUENT, the user has to define, amongst other smaller issues too many to mention:

- the boundary conditions (for the already selected boundary types in the pre-processor, GAMBIT);
- the use of the energy equation;
- the operating conditions (e.g., gravity, atmospheric pressure and temperature);
- the viscous model – laminar or turbulent, after which a suitable turbulence model must be chosen for the latter.

---

<sup>1</sup> The following references made use of typical CFD approaches to flow situations similar to that with the SEN and mould in the continuous casting process. Much of these references were a source of ideas and a guide to approaching the CFD modelling problem(s):  
[2][3][4][5][6][25][36][37][38][39][40][41][42][43][44][45][46][47][48][49]

All aspects, options and definitions must be carefully considered and specified by the user; otherwise default values will be used by FLUENT, possibly resulting in incorrect solutions if the flow requires specific value changes.

Initially, the author had no prior experience in modelling the very complex flow situation of the molten steel jet that enters the mould cavity. For a first iteration in an effort to obtain a first solution, default options for the flow of jets were chosen. As can be expected, a number of changes were necessary to obtain solutions that were representative of the real flow situation.

#### **4.1.2 Verifying base case CFD model**

Any CFD solution (usually required to make a design decision or some engineering judgement) should be verified in some way to ensure the solution is physically correct; otherwise the entire exercise will be meaningless. As mentioned in the Literature Survey, the most common verification method is a comparison with plant trials and/or water models. A model can be verified by only comparing certain significant measurements (key indicators), for example the impact point of the SEN jet(s) on the wall of the mould in this case. If these key indicators correspond closely, the CFD solution can be assumed to be correct, and other meaningful information can be extracted from the solution using post-processing<sup>2</sup> tools. E.g., the downward force on the SEN can be accurately computed using the CFD solution.

Most base cases in design optimisation exercises are based on the existing technology and/or application in the industry – several real ‘plant trials’ (or rather plant information) are thus available to the CFD modeller to validate the base case CFD model. However, in the case of the modelling in the SEN and mould, most

---

<sup>2</sup> Post-processing tools are usually included in the CFD code. In this dissertation, FLUENT has various tools, where forces, velocities, temperature distributions (to name but a few) can be computed from the solutions of the (adapted) Navier-Stokes equations and presented in the form of plots and/or contours (colour coded) on the desired geometries.

plant information only consists of mould temperatures and eventual defects in the processed product, e.g., hot rolled plate.

As anticipated, the first few solutions either did not converge towards a solution, or the solution was incorrect when compared to the literature and a full-scale water model. The process followed by the author to obtain a correct solution is best described in the diagram (Figure 4.1) in the section that follows. The process, as can be seen in Figure 4.1, involves a number of iterations to individually change settings in FLUENT and/or model geometry and gridding strategies (in GAMBIT) until a physically correct and converged solution is obtained.

#### **4.1.3 Summary: approach to base case CFD modelling**

Refer to Figure 4.1 for a summary of the approach followed by the author to obtain a satisfactory CFD solution for the base case.

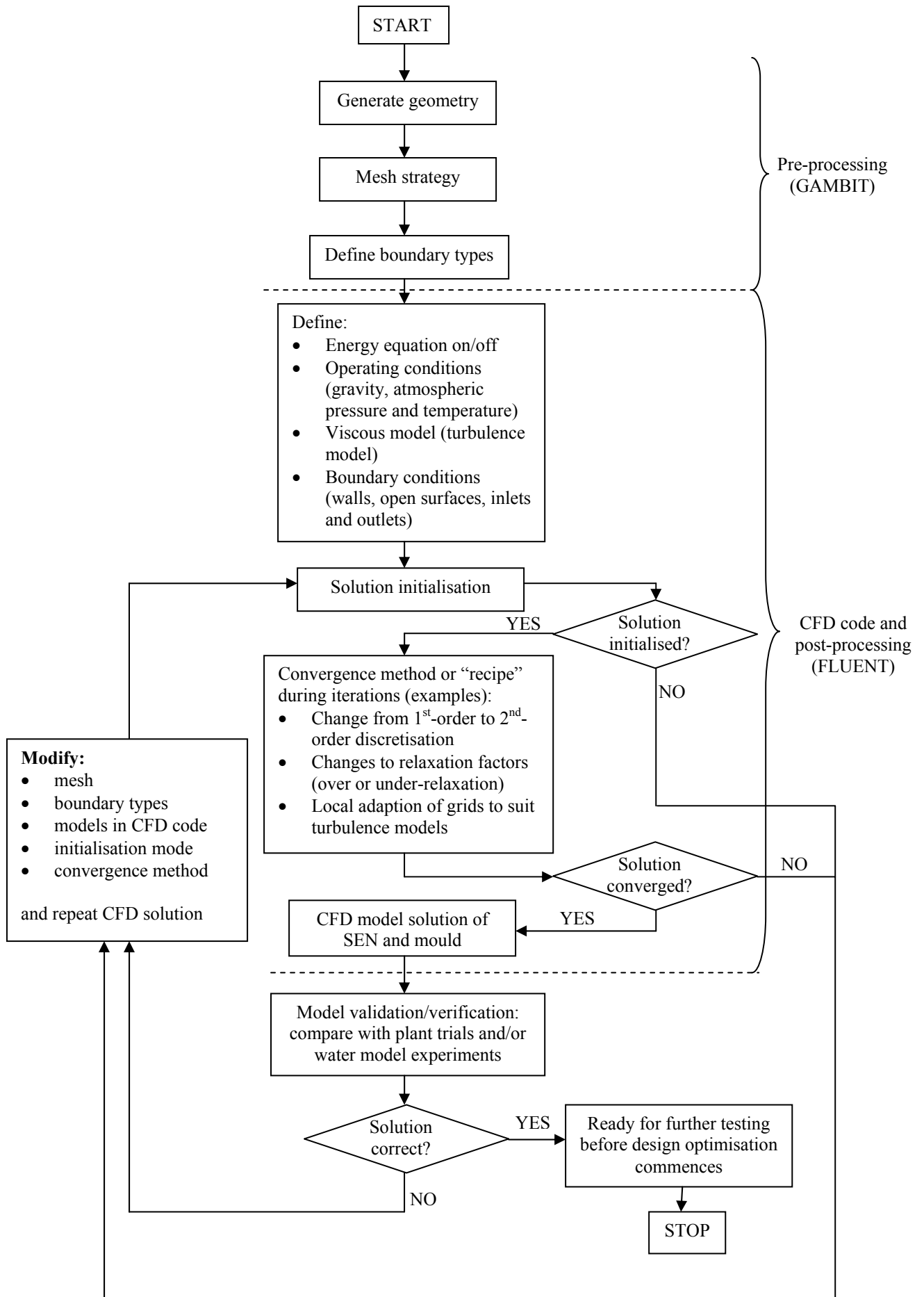


Figure 4.1: Diagram: Summary of the development of the base case CFD model

In the sections that follow, the specific gridding strategies used, choices made for turbulence models and boundary conditions will be discussed, and the reasons why they are preferred above other models and options will be stated accordingly. These choices of turbulence models, strategies, “recipes” and other options, will be repeated for other arbitrary SEN and mould designs for subsequent design optimisation exercises.

## 4.2 Description of base case

### 4.2.1 SEN description

The base case of this design optimisation exercise is the SEN currently<sup>3</sup> used at Columbus Stainless in Middelburg, South Africa.

The geometry of the base case SEN is shown in Figure 4.2. The Vesuvius<sup>®</sup> SEN has a bifurcated configuration, without a well, and the angle of the SEN ports are 15° upwards from the horizontal. The heights of the SEN ports are 70mm. The total length of the SEN is approximately 1.1m, and it tapers down from the top towards the nozzles, simultaneously morphing from a round cross sectional area to an almost rectangular cross sectional area. The submerged depth of the base case is 120mm, measured from the top of the nozzle port to the meniscus surface. However, during continuous casting, the submerged depth is varied from 80mm to approximately 200mm.

An extract of the drawings for the base case SEN design can be viewed in [Appendix G](#).<sup>4</sup>

---

<sup>3</sup> Currently refers to 2001/2002. Another SEN design, which comprises a well-type configuration, is to replace the current type without the well. Refer to [Appendix H](#) for the details and drawings.

<sup>4</sup> [Appendix G](#): Copyright: Vesuvius, South Africa.

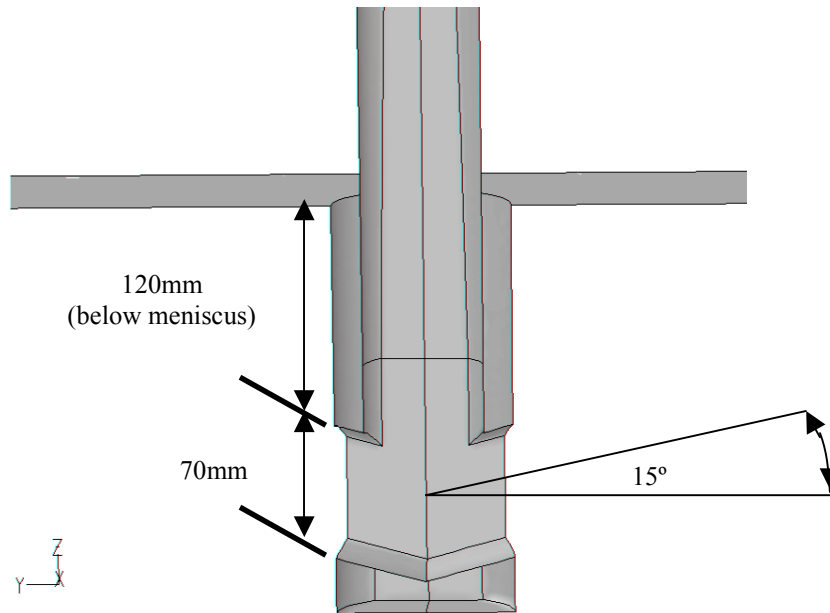


Figure 4.2: Basic geometry of base case SEN

#### 4.2.2 Mould description

For the base case, the width of the full-scale mould (and thus the slab width) is 1575mm. This is the width at which Columbus Stainless is experiencing the most quality problems. The thickness of the mould is 200mm. The mould is assumed to be rectangular, and the exact detail of the mould walls is thus neglected. Refer to section 4.3 in this chapter for more graphical information.

In the steel plant, the copper mould is approximately 800mm long, after which the solidified shell is extracted from the mould with water-cooled rollers. The slab (with shell that is solidified as it is cooled down) is then bent from a vertical orientation to a horizontal orientation through a curvature radius of approximately 9m, as explained in the Historical Development of Continuous Casting (Chapter 2). However, trial and error methods in previous work [2] have shown that if the curvature is neglected, and a total mould length of at least 3m is modelled, accurate and comparable results are obtained.

In this dissertation, the CFD modelling and the water model experimental set-up make use of this assumption, where a total mould length (includes roller-supported curvature in real steel plants) of 3 m (or more, where possible) is used.

#### **4.2.3 Momentum only vs. momentum and energy combined**

In an effort to validate the CFD model with water model experiments, the energy equation will be neglected, as cold water is used as the fluid in the CFD modelling. The effect of temperatures on the buoyancy of water is negligible in any event (the effect on liquid steel flow patterns is deemed to be not that influential [2]). However, after validation of the CFD model, the modelling fluid can easily be changed to liquid steel with associated temperature boundary conditions and energy equation modelling using FLUENT.

#### **4.2.4 Simultaneous SEN and mould modelling**

Unlike some other similar CFD work on SEN and moulds [2][3][4][5][6], the CFD model in this dissertation comprises the simultaneous solution of the SEN and mould, as the submergence of the SEN into the mould influences the resultant solution field.

In this dissertation (and optimisation work to follow), the SEN and mould will be simulated together in one CFD model for better correspondence with plant circumstances (and the water model). This complicates the flow field, especially at the nozzle ports as the flow exits into the mould. The importance of mesh quality at the nozzle exit ports will be discussed in more detail later in section 4.3.

When separating the SEN from the mould, solutions seem to be more stable and converge quickly to predetermined criteria. However, when evaluating the SEN



separately, a pressure outlet boundary condition is applied to the SEN where it exits into the mould cavity. The pressure will typically be assumed to be the ferrostatic pressure due to the submergence depth of the SEN below the meniscus. The flow is then solved and the velocity profile of the SEN exit nozzle is applied as a velocity inlet boundary for the mould in a separate simulation. Refer to Figure 4.3 for the location of the SEN outlet / mould inlet.

However, when measuring (in a SEN and mould combined CFD model after convergence) the pressure distribution on the SEN port face, a non-constant pressure distribution is observed. The static and dynamic pressure distributions are illustrated in Figure 4.4, and show that the pressure distribution is not constant or a linear pressure distribution. The dynamic pressure distribution in Figure 4.4(b) includes the effect of the jet kinetic energy (observed as a high total pressure in the region of high jet velocity). This proves the importance of evaluating the SEN and mould together in one CFD model, in an effort to capture the real physical flow situation.

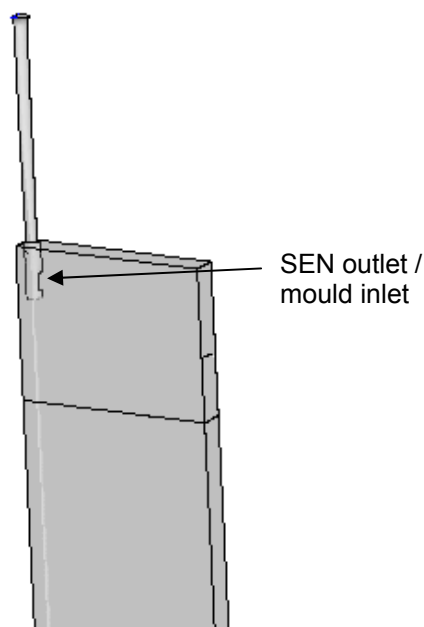


Figure 4.3: Location of SEN outlet port / mould inlet port (quarter model)

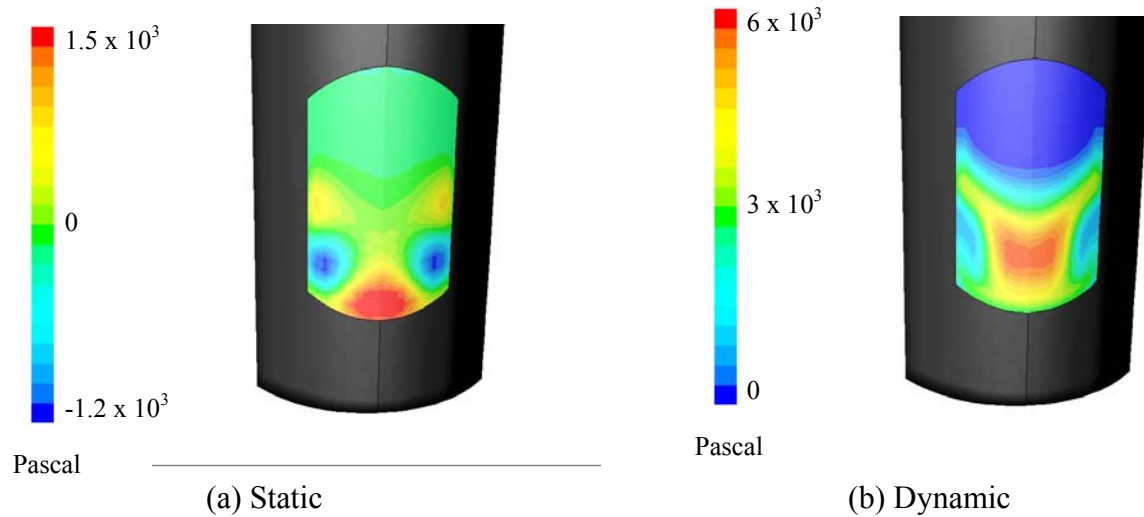


Figure 4.4: Static and Dynamic pressure distribution in 3D SEN port face (quarter model) in Pascal

#### 4.2.5 2D and 3D modelling

Although 3D CFD modelling will be much more representative of the physical flow situation in the SEN and mould, 2D models are also developed alongside the 3D models. The main reason is the fact that 3D CFD models are much more computationally expensive than 2D models. If the 2D CFD model solutions are similar to that of 3D (and there are many similarities – refer to section 4.4.2), it would be much more sensible to perform design optimisation with 2D models.

Thus, throughout this dissertation, there will be made use of both 2D and 3D CFD models and, when compared, differences will be pointed out and explained.

### 4.3 CFD set-up

#### 4.3.1 Geometry and gridding strategy (pre-processing)

##### **Symmetry assumed:**

In this dissertation, the flow is assumed to be symmetrical. A half model is therefore used for the 2D model, and a quarter model for the 3D model. However, due to small flow differences experienced in continuous casting plants and the water model, the flow will never be completely symmetrical in practice. The water model results proved this fact (refer to Chapter 3, section 3.3 where the asymmetrical flow field is shown in Figure 3.12). The overall geometry (flow area) can be seen in Figure 4.5, where the 3D quarter model is shown without the mesh to indicate boundary conditions.

##### **Importance of element types:**

Trial and error methods have proven that the element types chosen have a significant effect on the solution: not only the end result, but also the manner (stability, numerical errors amongst others) in which the solution approaches convergence.

Initially, in order to accommodate later optimisation parameterisation, the volume around the nozzle area was meshed using an unstructured grid (tetrahedral elements or volumes). The author used this method as the mentioned volume (refer to Figure 4.6) will change if the typical nozzle parameters (port height, port angle for example) change, and unstructured (tetrahedral) grids are automatically generated by the pre-processor GAMBIT for rather complicated volumes. However, the most complex flow is found at the SEN nozzles, where the jets exit into the mould cavity. Subsequently, incorrect flow patterns regularly (but not always) were observed using unstructured grids at the critical and unstable jet orifices.

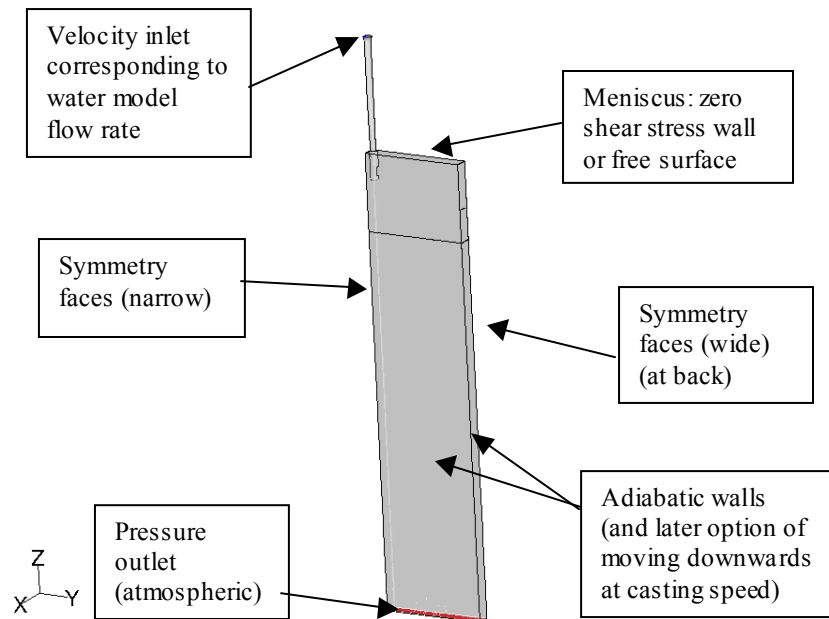


Figure 4.5: Typical boundary conditions for momentum-only CFD model validation (quarter model)

In collaboration with another university<sup>5</sup> also modelling different flow situations in continuous casting using CFD, it was found that hexahedral cells proved to deliver much more reliable and repeatable solutions. Accordingly, the volume shown in Figure 4.6 has to be divided into smaller volumes that can be meshed with hexahedral cells or elements.

<sup>5</sup> University of Illinois at Urbana-Champaign

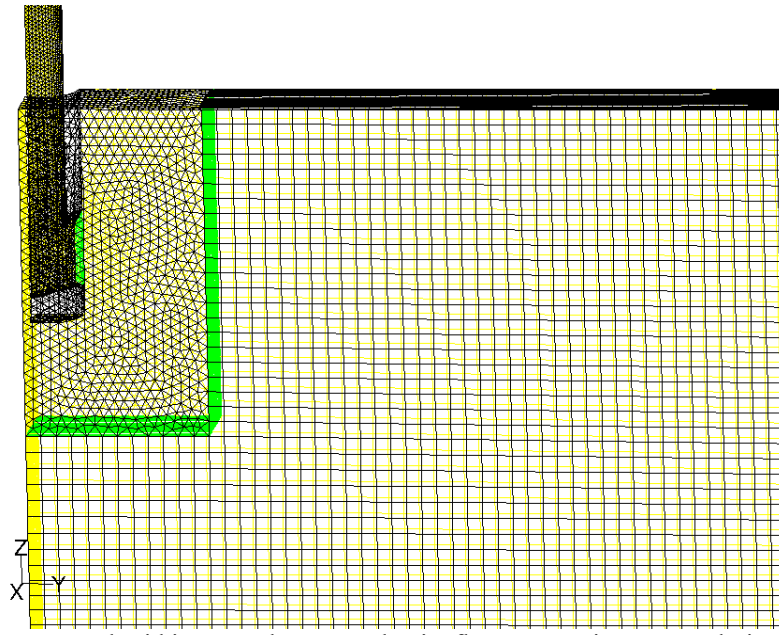


Figure 4.6: Unstructured grid in area where complex jet flow occurs: incorrect solutions often result (quarter model, 3D)

Figure 4.7 shows a zoomed-in view (from the back) of the same volume that is divided into simpler volumes, which can be meshed using hexahedral cells. The nozzle volumes (inside the lower part of the SEN) also needed to be divided into simpler volumes to enable exclusive hexahedral cells meshing.

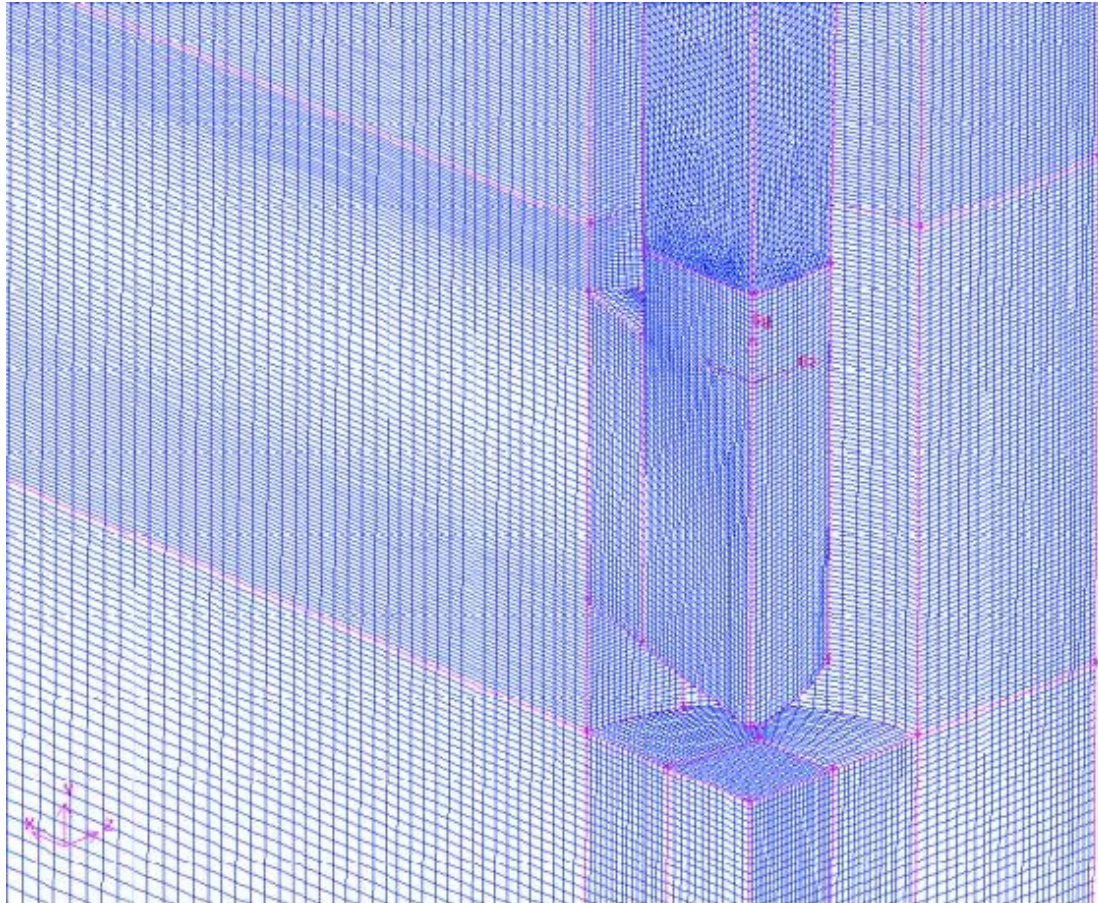


Figure 4.7: Structured grid (hexahedral cells) in complex flow area results in more repeatable solutions (quarter model, 3D)

The SEN shaft morphs from a circular cross section to a partly rectangular cross section. This fact causes a sharp edge in the quarter model of the geometry, forcing one to make use of tetrahedral cells in a small volume about this sharp edge. Unfortunately, these tetrahedral cells have a detrimental effect on the flow field, upsetting the uniform flow inside the SEN shaft just before being directed by the SEN nozzles into the mould cavity.

*Virtual geometry enables exclusive hexahedral meshing*

The solution to this mesh problem was to make use of FLUENT's virtual geometry and meshing capabilities [10]. Before meshing the volume about the sharp edge, a virtual<sup>6</sup> modification is made to the geometry. Virtual hexahedral

---

<sup>6</sup> "Virtual" suggests that the modification is not made to the real volume or geometry. The pre-processor (GAMBIT) performs a superficial modification to enable a more stable mesh, without altering the basic geometry.

cells are then generated within the virtual geometry. Subsequently, the entire 3D model of the SEN and mould can be meshed with the exclusive use of hexahedral cells, which, as trial and error has proven, is essential for correct and repeatable CFD results.

The use of virtual volumes and virtual hexahedral cells was also incorporated in the GAMBIT script file (for automatic geometry and mesh generation) in Chapter 5, during the design space exploration as an optimisation exercise to find an optimum 3D SEN design.

Similar problems also occurred in 2D modelling: subsequently quadrilateral elements are used instead of unstructured pave elements. This was achieved by dividing all areas with 5 or more sides (polygons) into quadrilateral areas or cells, before attempting to mesh the geometry.

#### 4.3.2 **Boundary conditions**

The typical boundary conditions specified in the CFD model for the base case are shown in Figure 4.5 above. The 2D boundary conditions are similar to that of the 3D model.

##### **Meniscus boundary condition:**

The meniscus boundary condition (see Figure 4.5 above) can either be a zero shear stress wall, or a free surface with a volume air generated above the latter. Using the Volume of Flow (VOF) method in FLUENT, the behaviour of the free surface (meniscus) and the influence on the flow solution inside the mould was evaluated. The VOF-method required very expensive unsteady solvers: thus only a 2D simulation was evaluated. The mould flow fields compared favourably (refer to [Appendix I](#)); consequently the less expensive boundary condition (zero shear stress wall or slip wall which simulates a free surface) will be used for later optimisation studies and for the base case CFD model validations in this chapter. Moreover, it is currently much easier to extract heat from the meniscus by simply

specifying a heat flux boundary condition. However, in possible future work when the exact behaviour of the meniscus becomes important, the use of the VOF-method (or something similar) will be a necessity.

**Velocity inlet:**

The velocity inlet, specified as perpendicular to the inlet boundary, corresponds to the water model flow rate. Later, it can easily be correlated with the steel mass flow rate taking into account the density of the steel to be cast. The stopper of the tundish (which is also modelled in the water model – refer to Chapter 3), which controls the flow to the mould, is taken into account in the CFD model by modelling the inlet boundary as an annular inlet.

**Symmetry faces:**

The assumption of symmetry in the width and thickness of the mould allows one to only model a quarter of the SEN and mould (3D model). The solution is thus assumed to be identical in all four quarters. By defining two symmetry planes, FLUENT can solve the entire mould model – by only solving a quarter model.

**Mould walls:**

*Adiabatic walls (only for model verification purposes):*

For the purpose of the base case CFD model validation, the walls will be considered to be adiabatic and stationary. However, the model can easily be altered to move the walls at casting speed and with a liquidus temperature imposed, to more closely simulate plant conditions for later optimisation evaluations.

*Walls at liquidus temperature: (for model of steel plant):*

As soon as the CFD model of the base case is verified using the water model results, it is easy to alter the boundary conditions of the walls in FLUENT. The boundary conditions on the mould walls will include the following settings:

- walls at liquidus temperature (1450 °C)
- walls moving downwards at casting speed (1.0 m/min for base case)



- heat flux from the flow field in the copper mould contact area and from meniscus (approximately  $300\,000\text{W/m}^2$ , which must be converted for 2D models)

Owing to the fact that only thick slab casting is considered in this work, it is assumed that the shape of the solidifying shell does not influence the fluid flow, as the walls are assumed to be straight. However, the author is aware that shell forming may have a profound influence on the flow patterns with thin slab casting, which is beyond the scope of this work.

Subsequently, only single-phase flow will be evaluated in the mould volume, as it is assumed that solidification does not take place.

#### **Pressure outlet (atmospheric):**

Trial and error methods have proven that the use of an atmospheric pressure outlet results in more physically correct solutions, than using an outflow (zero gradient) outlet. As the steel solidifies in the strand, the correct choice of boundary conditions is difficult. Rather, this boundary location is chosen to be far enough away, in such a way not to influence the flow patterns around the SEN. At first, a mould length of 3m was used and deemed to be far enough away; however, with later 3D design exploration models (refer to Chapter 5, section 5.6), a mould or rather strand length of 4.3m was used, with much success<sup>7</sup>.

### **4.3.3 CFD options and assumptions**

#### **Steady-state:**

The steady-state solution for the CFD flow field is required in order to compare with the water model – it is assumed that the water model has reached a steady flow field as soon as the meniscus level is stable (when the dye is injected – refer to Chapter 3 for more information).

---

<sup>7</sup> Solutions were more stable and converged faster due to lack of excessive backflow through the mould exit.

However, some SEN designs caused a very unstable simulated flow field, where the jets never really stabilised, but rather fluctuated around an average jet position. This unsteady behaviour was mostly noticed on 3D CFD models with wide widths (1575mm), and thus did not severely influence the optimisation studies in Chapter 5. Some recommendations for future work concerning unsteady flow fields are discussed in Chapter 6.

**Operating conditions:**

Operating conditions include specifying the

- atmospheric pressure (which can of course be lower than 101.3 kPa depending on height above sea level);
- surrounding atmospheric temperature; and the
- gravity vectors (depending on orientation of model).

**Turbulence model:**

A jet exiting into a larger cavity (such as the SEN nozzle exiting into the mould) definitely suggests turbulent flow [9]. FLUENT offers a number of viscous and turbulence models to suit most flow problem types. Whenever a turbulent flow situation is anticipated, the k- $\epsilon$  turbulence model is usually implemented because of its adequate accuracy (in most circumstances) as opposed to relative little computing time.

Whenever more accurate turbulent models are implemented, such as Large Eddy Simulation (LES) or the Reynolds Stress Model (RSM), a considerable increase in computing time is required. With LES, an extremely fine mesh is necessary to successfully use this sub-grid scale turbulence model [38]. With RSM, on the other hand, 7 equations must be solved for each cell every iteration for 3D (as opposed to the k- $\epsilon$  model's 2 equations).

FLUENT compares the relevant turbulence models as follows (Table 4.1):

Table 4.1: Comparison between different turbulence models [10]

Model	Strengths	Weaknesses
<b>Standard k-<math>\epsilon</math></b>	Robust, economical, reasonably accurate; long accumulated performance data	Mediocre results for complex flows involving severe pressure gradients, strong streamline curvature, swirl and rotation
<b>RNG<sup>8</sup> k-<math>\epsilon</math></b>	Good for moderately complex behaviour like jet impingement, separating flows, swirling flows, and secondary flows	Subjected to limitations due to isotropic eddy viscosity assumption
<b>Realisable k-<math>\epsilon</math></b>	Offers largely the same benefits as RNG; resolves round jet anomaly however	Subjected to limitations due to isotropic eddy viscosity assumption
<b>Reynolds Stress Model (RSM)</b>	Physically most complete model of large and small-scale turbulence (history, transport, and anisotropy of turbulent stresses all accounted for); isotropy not assumed	Requires more CPU effort (2 to 3 times more than k- $\epsilon$ methods); tightly coupled momentum and turbulence equations
<b>Standard k-<math>\omega</math><sup>9</sup></b>	Apart from similar strengths as Standard k- $\epsilon$ model, it incorporates low Re-number effects and shear flow spreading. Applicable to wall-bounded flows and free shear flows.	Subjected to limitations due to isotropic eddy viscosity assumption. Also marginally more expensive due to more built-in models and sophistication for specific flow circumstances.
<b>SST k-<math>\omega</math></b>	Blend robust and accurate formulation of k- $\omega$ model in near-wall regions with free stream independence of k- $\epsilon$ in far field. More accurate and reliable for wider class of flows, <i>i.e.</i> , adverse pressure gradient flows (e.g., airfoils), transonic shockwaves, etc.	Subjected to limitations due to isotropic eddy viscosity assumption
<b>Large Eddy Simulation (LES)</b>	Models small-scale turbulence directly; no assumptions on flow	Requires extremely fine mesh and (mostly) exclusive hexagonal

<sup>8</sup> RNG: Renormalisation Group Method. This k- $\epsilon$  method encompasses the standard k- $\epsilon$  equations, with the addition of applying a rigorous statistical technique [10].

<sup>9</sup> Addition to turbulence models available in FLUENT since 2003

	conditions	(structured) grids. Subsequently ridiculously computationally expensive and not suited for optimisation work.
--	------------	---

Trial and error methods proved that the choice of a turbulence model has a radical effect on this particular flow field. The flow field is sensitive to the combination of turbulence model, mesh quality and solution procedure followed. For this dissertation, the RSM model was selected for some 3D simulations owing to its better grid independence (as opposed to the  $k-\epsilon$  model). The RSM model is further more accurate in predicting real turbulent 3D flow fields, as turbulent velocity fluctuations around a time-averaged mean velocity is computed by solving transport equations for each of the terms in the Reynolds stress tensor [10]. The family of  $k-\epsilon$  and  $k-\omega$  models assume turbulent fluctuations to be the same in all directions (isotropic turbulence – also see Table 4.1). The anisotropic nature of turbulence in highly swirling flows and stress-driven secondary flows has a dominant effect on the mean flow situation – therefore RSM is clearly the superior model for the SEN and mould model [10].

The cost of RSM however disqualified it for use in an optimisation environment, where many simulations need to be performed. The base case SEN design (with a submergence depth of 200mm, however) was modelled using the RSM turbulence model. The mesh consisted of approximately 3 million cells. In order to ensure convergence, the CFD model iterated for several months on a 3 GHz Intel Pentium 4, reaching approximately 44 000 iterations. This proves that the RSM turbulence model is not suitable for general optimisation use with current computational power.

However, since the addition of the  $k-\omega$  turbulence model to FLUENT in 2003 [10], this much less expensive 2-equation model proved to be well suited for jet-like flows. The Standard  $k-\omega$  model is based on the Wilcox  $k-\omega$  model [50]. Both  $k-\omega$  turbulence models (Standard (STD) and Shear Stress Transport (SST)) [51] incorporate modifications for low Re-number effects, compressibility, and shear flow spreading. Wilcox's model predicts shear flow spreading rates that are in close agreement with

measurements for far wakes, mixing layers, as well as plane, round and radial jets. These models are thus applicable to wall-bounded flows and free shear flows.

The Standard  $k-\omega$  model proved to be most suited for 3D CFD models of the SEN and mould. This turbulence model was also used successfully in Chapter 5, section 5.6, during a design space exploration optimisation exercise for specifically 3D SEN and mould models.

On the other hand, 2D modelling proved to be accurate with the  $k-\varepsilon$  Realisable model [39]. Although this model also assumes isotropic turbulence, the effect on the mean flow is negligible in 2D modelling. The  $k-\varepsilon$  Realisable model (as opposed to the Standard  $k-\varepsilon$  model) is more suited for flow features that include strong streamline curvature, vortices, rotation and complex secondary flow features (see Table 4.1).

#### Near-wall treatments:

Most  $k-\varepsilon$ ,  $k-\omega$ , and RSM turbulence models will not predict correct near-wall behaviour if integrated down to the wall. For this reason, so-called wall functions need to be used in conjunction with these turbulence models to empirically predict the correct transition from the fully turbulent region to the laminar viscous sub layer. FLUENT compares three near-wall treatments to be used in conjunction with any of the turbulence models discussed above (Table 4.2):

Table 4.2: Comparison between different near-wall treatments [10]

Wall functions	Strengths	Weaknesses
<b>Standard wall functions</b>	Robust, economical, reasonably accurate	Empirically based on simple high Re-number flows; poor for low Re-number effects, $\nabla p$ , strong body forces, highly 3D flows
<b>Non-equilibrium wall functions</b>	Accounts for $\nabla p$ effects, allows non-equilibrium for: separation, re-attachment and impingement	Poor for low Re-number effects, massive transpiration, severe $\nabla p$ , strong body forces, highly 3D flows

Wall functions	Strengths	Weaknesses
Two-layer zonal model	Does not rely on law-of-the-wall, good for complex flows, especially applicable to low Re-number flows	Requires finer mesh resolution and therefore larger CPU and memory resources

Although Table 4.2 suggests that non-equilibrium wall functions should be superior to standard wall functions, trial and error methods proved that no significant advantage was obtained using the former. Either of the wall function treatments can thus be used for the current application. Note that the two-layer zonal model was not even considered, as it is more appropriately used with low Re-number flow fields.

The use of quadrilateral elements (2D) and hexahedral cells (3D) is advised at the boundaries for more accurate results using wall functions. In order to ensure that the wall functions predict correct near-wall flow, the cell (or element) size needs to be chosen correctly: this is checked periodically during the solution procedure – refer to section 4.3.4 below for more detail.

#### Other settings:

Depending on the software used, different settings are required for highly swirling flows and jets. Constants in the models and equations were tuned specifically for this flow field as suggested by the CFD software and trial and error methods to stabilise the flow. Noteworthy areas not mentioned in the discussion above include:

- pressure discretisation scheme settings (PRESTO! and body weighted schemes proved to be the most suited for the SEN and mould modelling [10])
- solution criteria monitor settings
- solution procedures (*i.e.*, under-relaxation factors, ‘recipe’ of changing from first-order discretisation to second-order discretisation – see section 4.3.4 in this chapter).

#### 4.3.4 Solution Procedure

##### *Initialisation:*

During the iteration process, certain milestones must be reached before switching to more accurate solver algorithms. For example, before the iteration process can commence, an initial solution must be guessed. This initial estimate of a flow field can thus be seen as a first milestone before the iteration process can begin.

##### *1<sup>st</sup>-order and 2<sup>nd</sup>-order discretisation schemes:*

Due to the nature of the numerical solution of the discretised Navier-Stokes equations, the solution needs to “propagate” from the inlet boundary through the SEN into the mould cavity. In order to speed up this process, the first few hundred iterations (may differ immensely depending on type of grid, 2D or 3D, type of turbulence model, etc.) are performed with first-order discretisation.

As the first-order solution approaches convergence, the second-order discretisation scheme is enabled, using the solution of the first-order scheme as an initial solution from which to iterate. When the second-order solution has converged, it is assumed to be the solution to the initial CFD problem.

##### *Under- and over-relaxation factors:*

As explained in the Literature Survey (Chapter 2, section 2.3.4.2), it is often necessary to adjust the over-relaxation factors to prevent the non-linear Navier-Stokes equations from diverging. Under-relaxation comprises the slowing down of changes from iteration to iteration. Over-relaxation (accelerating these changes) is often used to test whether a “converged” solution is indeed converged and stable.

However, trial and error methods have indicated that a certain ‘recipe’ or rather procedure is required to ensure convergence of SEN and mould CFD problems. It is necessary to adjust the under-relaxation factors every few hundred iterations (see below for solution procedure and Figure 4.8) to ensure that the residuals converge sufficiently. As soon as the solution seems to be nearing convergence (also comparing real flow indicators monitored during the iteration procedure), the

relaxation factors can be adjusted upwards (towards over-relaxation) to ensure a true converged solution.

*Wall functions – grid adaption necessary:*

In order for the wall functions (described in section 4.3.3) to predict the near-wall flow correctly, the grid cells adjacent to the wall need to be sized correctly. The size is determined by the  $y^+$ -value of that cell: the  $y^+$ -value of a cell is a function of the velocity of and the properties (density, viscosity *inter alia*) of the fluid in that cell, and is in fact a local Reynolds number based on the friction velocity and the normal spacing of the first cell. For the  $k$ - $\epsilon$  and  $k$ - $\omega$  turbulence models, the wall function approach requires the  $y^+$ -value to be between 50 and 500 [dimensionless].

Whenever reverse flow is experienced over any boundaries in a CFD model, the situation may arise that mass imbalances occur. The SEN and mould CFD model is an example where mass imbalances occur: due to a recirculation zone in the mould, reverse flow is experienced over the pressure outlet boundary. These mass imbalances must be periodically rectified during the solution procedure using grid adaption (refer to the solution procedure below).

*Grid adaption and virtual meshes:*

Whenever virtual meshes are required and used (for 3D mesh of SEN and mould), normal grid adaption during solution iterations is not possible. Consequently, grid adaption due to mass-imbalances is also not possible.

*Dynamic grid adaption:*

However, a new feature added to FLUENT (FLUENT 6.1.1. [10]) enables the user to dynamically adapt the virtual grid during the solution procedure. Starting (since initialisation) from an initial mesh size (typically 500 000 cells for this 3D case), the mesh is refined and coarsened as the solution proceeds, based on velocity gradients (other criteria can also be used). This is an attempt to follow the formation of the SEN jet with grid clustering. A maximum cell count of approximately 850 000 is reached in this process depending on the complexity of



the flow field and the SEN geometry used (part size, number of design parameters, etc.). The dynamic mesh adaption option is chosen and configured before the solution iteration process is started, and dynamically adapts the mesh as the solution proceeds until sufficient convergence is achieved.

*Other solution procedure settings:*

Different functions and schemes can be switched on and off during the solution procedure to aid the solution to meet the convergence criteria as soon as possible. Obviously, these setting changes can only be performed when the iteration procedure has been interrupted. Over-zealous interruptions and setting changes can have a negative impact on the convergence and subsequent correctness of the CFD solution.

The (typical) solution procedure used to obtain the results displayed in section 4.4 is shown below. Refer to Figure 4.8 for the graphical presentation of the solution procedure, using the residuals.

The **solution method** or **procedure** comprises:

*First-order solution*

1. Run 300 iterations
2. Adapt (refine) grid as follows:
  - $y^+$  values at walls: ensure that  $50 < y^+ < 200$
  - mass-imbalance: ensure that  $-10^{-5} < mi < 10^{-5}$
3. Run 300 iterations
4. Adjust under-relaxation as follows:
  - pressure correction equation:
 

p	=	0.2	(from default 0.3)
---	---	-----	--------------------
  - momentum equation:
 

mom	=	0.5	(from default 0.6)
-----	---	-----	--------------------
  - turbulence kinetic energy equation:
 

k	=	0.6	(from default 0.8)
---	---	-----	--------------------
  - $\varepsilon$  equation (from k- $\varepsilon$ )
 

$\varepsilon$	=	0.6	(from default 0.8)
---------------	---	-----	--------------------
5. Run 100 iterations

6. Adapt grid for mass-imbalance
7. Run 250 iterations
8. Under-relaxation as follows:
 

momentum:	mom	=	0.4	(from 0.5)
-----------	-----	---	-----	------------
9. Run 400 iterations

*Second-order solution*

10. Change all settings to second-order, except pressure discretisation method (set this to body weighted or PRESTO!)
11. Run 150 iterations
12. Unrelax in order to ensure correct solution as follows:
 

pressure correction:	p	=	0.3	(from 0.2)
momentum:	mom	=	0.6	(from 0.4)
13. Run 400 iterations
14. Adapt grid for mass-imbalance
15. Run 150 iterations
16. Under-relax as follows:
 

momentum:	mom	=	0.5	(from 0.6)
-----------	-----	---	-----	------------
17. Run 350 iterations
18. Tighten the convergence criteria for momentum to 0.00075 (from 0.001)
19. Under-relax as follows:
 

momentum:	mom	=	0.4	(from 0.5)
-----------	-----	---	-----	------------
20. Run 300 iterations
21. Under-relax as follows:
 

momentum:	mom	=	0.375	(from 0.4)
-----------	-----	---	-------	------------
22. Run 1000 iterations (until convergence which mostly occurred before 700 iterations)

(Total number of iterations = 2250 to 2850, depending on convergence occurrence in step 22)

Note that whenever an adjustment to any of the CFD code settings is made (relaxation factor adjustment to discretisation scheme adjustment), the residuals spike momentarily (refer to Figure 4.8).

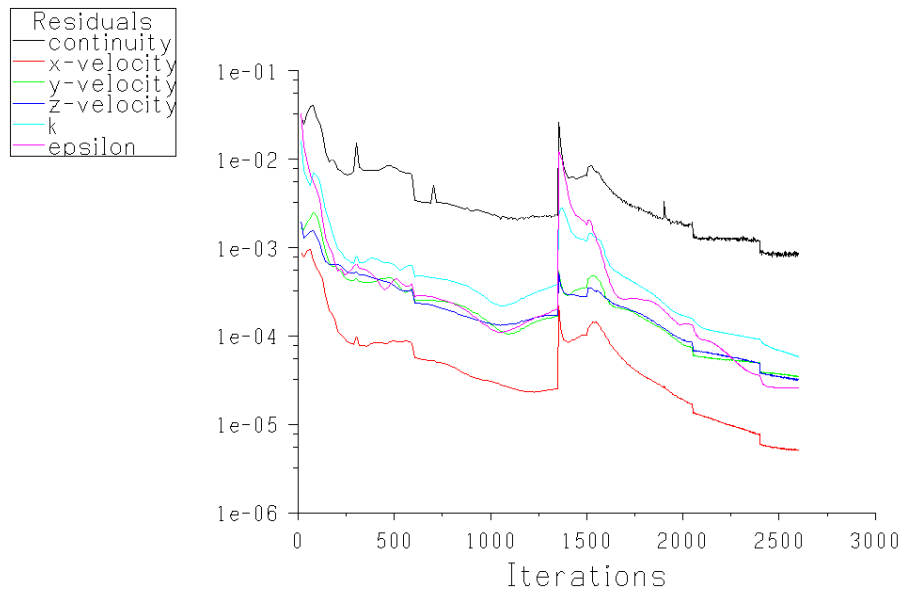


Figure 4.8: Residuals during solution procedure ('recipe')

## 4.4 CFD model: Verification Results

### 4.4.1 CFD model verification: mimic water model

The reason as to why a water model was designed and built by the University of Pretoria (the author) was to validate the CFD model of the SEN and mould before any design optimisation is attempted.

The first step to validate the model is to concentrate on the flow patterns only (momentum only), by exactly imitating the 40%-scaled water model. If the CFD momentum model closely matches the flow patterns of the 40%-scaled water model, the model<sup>10</sup> can be assumed to be acceptable.

From here, it is rather a straightforward exercise to extend the model to imitate real plant circumstances, by scaling the geometry to full-scale, enabling the

<sup>10</sup> The CFD "model" includes all aspects covered in Figure 4.1, and briefly includes geometry and gridding strategy, flow assumptions, CFD options and CFD assumptions, boundary conditions, and finally the solution procedure.

energy equation (and therefore allow temperature and buoyancy effects), and adjusting and supplementing the boundary conditions. Refer to section 4.5 for these actions. It should however be stressed that a high-fidelity modelling of the plant situation (e.g., modelling of mould oscillation, solidification, conglomeration of inclusions, etc.) falls outside the scope of this dissertation.

#### 4.4.1.1 Case 1: Base case (Old SEN of Columbus Stainless)

In summary, the following operating parameters and/or settings were selected for this CFD simulation:

- Base case SEN design as described in section 4.2, scaled to 40% in FLUENT to match the water model
- Energy equation disabled: only momentum equations considered
- CFD options:
  - k- $\epsilon$  realisable turbulence model for 2D
  - standard wall function
  - symmetry assumed (half model for 2D and quarter model for 3D)
- Boundary conditions: (refer to Figure 4.5)
  - Casting speed: inlet SEN velocity scaled to exactly match Fr-similarity flow rate of 1.72 m<sup>3</sup>/h (refer to Chapter 3 for details)
  - Meniscus: zero shear stress wall
  - Mould walls: adiabatic (by default) and stationary
  - Outlet at atmospheric pressure
- Material properties:
  - Water at 998 kg/m<sup>3</sup>
  - Other properties of water at Standard Temperature and Pressure

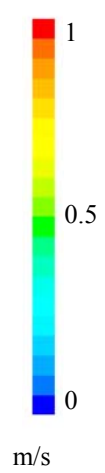
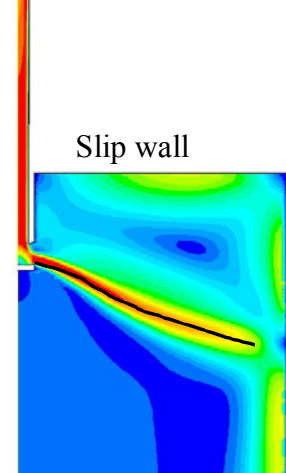
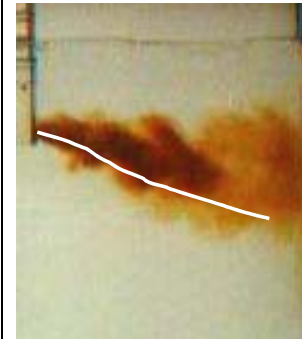
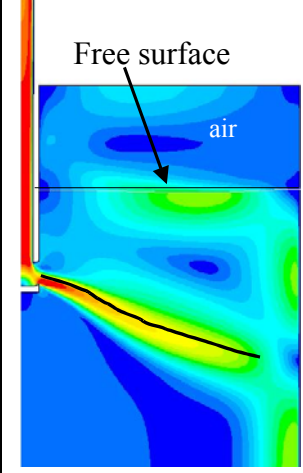
For the validation purposes of the CFD model, the submergence depth was modelled at 200mm (as opposed to the 120mm in the original base case), as several water model tests had already been performed at 200mm submergence.

Refer to Table 4.3 for the comparison of the 2D CFD model with the water model results. For the sake of completeness, the 2D results (Table 4.3) where the meniscus boundary was evaluated as a free surface (as opposed to a less expensive slip wall) are also shown to demonstrate the favourable comparison (also see Appendix I).

It can be seen that the 2D CFD model predicts a jet that penetrates deeper than observed in the water model. The intensity of the 2D simulated jet seems to be higher than that of the water model, *i.e.*, higher velocities are concentrated on the centreline of the simulated jet, as opposed to the more dissipated nature of the water model jet. The same trend is also observed when comparing simulated 2D and 3D results, with the 3D results being more representative of the water model observations.

The CFD results in Table 4.3 are displayed in the form of contours of velocity magnitude, just to highlight the flow pattern (momentum only) for validation purposes.

Table 4.3: Verification of 2D CFD model (slip wall and free surface meniscus boundary condition) with 40%-scaled water model. CFD results displayed using contours of velocity magnitude

CFD Scale	2D: zero shear stress (slip) wall meniscus	UP 40% Water model	2D: free surface meniscus
 m/s	 Slip wall		 Free surface air
<b>Base case (Old SEN): Submergence 80mm (200mm full-scale); Fr-similarity 1.72m<sup>3</sup>/h</b>			

#### 4.4.1.2 Case 2: New SEN of Columbus Stainless

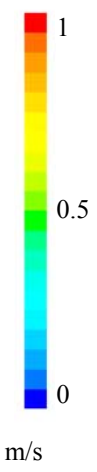
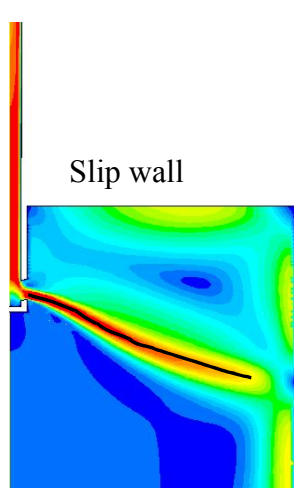
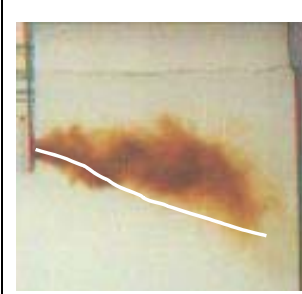
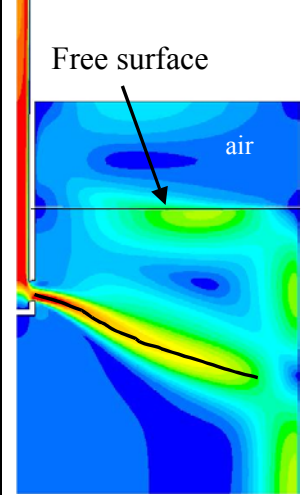
Columbus Stainless also requested water model testing of their more recent SEN design. Subsequently, the author was in possession of another case (physical SEN insert for the water model experimental set-up) to verify the CFD model of the SEN and mould.

The parameters and/or settings were identical to that of the base case (Old SEN), except for the different SEN design. The new design has the following parameters: (refer to [Appendix H](#) for drawings of new SEN design)

- port angle: 15° upward
- port height: 60 mm
- port width and radii: 45mm and 35mm (similar to base case design)
- well depth: 15mm
- well angle: flat

Refer to Table 4.4 (below) for the comparison of the 2D CFD model of the New SEN with the 40%-scaled water model results.

Table 4.4: Verification of 2D CFD model (slip wall and free surface meniscus boundary condition) with 40%-scaled water model. CFD results displayed using contours of velocity magnitude

CFD Scale	2D: zero shear stress (slip) wall meniscus	UP 40% Water model	2D: free surface meniscus
 1 0.5 0 m/s	 Slip wall		 Free surface air
<b>New SEN: Submergence 80mm (200mm full-scale); Fr-similarity 1.72m<sup>3</sup>/h</b>			

Again, it can be seen that the 2D CFD model predicts a jet that penetrates deeper than that observed in the water model. The line drawn inside the jet (all three figures in Table 4.4) corresponds closely to the concentrated jet of the 2D CFD solutions, indicating the more dissipative jet of the water model.

#### 4.4.2 2D vs. 3D verification results

##### 4.4.2.1 3D verification results

*Settings:*

Apart from extending the 2D CFD model settings and parameters to 3 dimensions, the turbulence model choice had to be altered:

As trial and error methods have proven, the k-ε turbulence models are not suited for 3D modelling. Consequently, as explained in section 4.3.3, the rather expensive RSM turbulence model was selected for this validation study. However, it was soon realised that the RSM turbulence model is too

computational expensive for general optimisation purposes, as it also demands a fine mesh (in excess of 2 million cells), apart from the fact that it requires 7 equations to be solved per iteration (as opposed to only 2 of the  $k$ - $\epsilon$  models). The result displayed in Table 4.5 has run for 52000 iterations, taking several months on a 3GHz Pentium IV with 2GB RAM computer to complete.

The less expensive Standard  $k$ - $\omega$  turbulence model (also only 2 equations per iteration) was selected as the turbulence model for the 3D model of the steel plant (section 4.5), which proved to be a good assumption, especially for smaller width moulds.

Refer to the Table 4.5 for the comparison between the 3D models of both turbulence models ( $k$ - $\omega$  and RSM) on the base case SEN design, and the 40%-scaled water model. The contours of velocity magnitude on the symmetry plane (*i.e.*, centre plane of the mould) of the CFD models are displayed. Note that both CFD models were configured to exactly imitate the 40%-scaled water model test.

*Note on Table 4.5: differences between 3D CFD models and water model results*

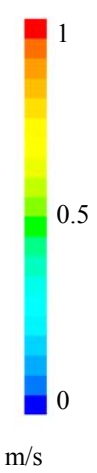
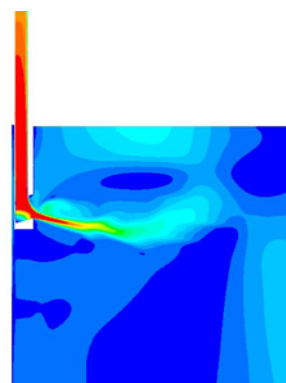
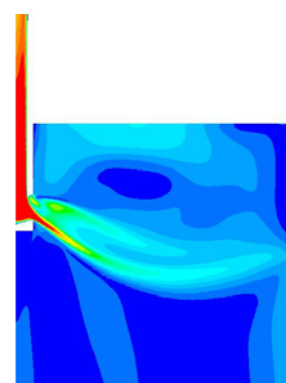

There is a noticeable difference between the 3D CFD models ( $k$ - $\omega$  and RSM turbulence closure) and the 40%-scaled water model. As more experience in SEN 3D modelling was gained during this study, it was noticed that the wider widths presented problems for most CFD methods. For example, the residuals struggled to fall below 3<sup>rd</sup>-order convergence. Moreover, the flow field seem unstable and pseudo-transient, although otherwise suggested by water model experiments. Furthermore, the pseudo-transient nature of the results seems to worsen as soon as 2<sup>nd</sup>-order upwinding is introduced.

Nevertheless, later 3D optimisation work in Chapter 5 was conducted on narrower slab widths (range 1000 – 1300mm), and the 3D CFD models



employing k- $\omega$  (standard) turbulence closure proved to closely simulate water model verification experiments (refer to Chapter 5, Figure 5.19).

Table 4.5: Verification of base case 3D CFD model (comparing RSM and k- $\omega$  (standard) as turbulence models) with 40%-scaled water model; 1575mm full-scale width. CFD results on quarter model centre plane displayed using contours of velocity magnitude

CFD Scale	3D centre plane RSM turbulence model, 2 <sup>nd</sup> -order accuracy	3D centre plane k- $\omega$ (standard) turbulence model, 2 <sup>nd</sup> -order accuracy	UP 40% Water model
 1 0.5 0 m/s			
<b>Base case (Old SEN): Submergence 80mm (200mm full-scale); Fr-similarity 1.72m<sup>3</sup>/h</b>			

4.4.2.2 Differences between 2D and 3D CFD models of SEN and mould

Comparing the CFD results in Tables 4.3, 4.4 and 4.5, the 3D flow pattern of the vertical section through the mould centre parallel to the wide face (*i.e.*, centre plane) can be reasonably approximated with the 2D model, also as pointed out by Thomas [2]. The only significant difference between the two flow patterns is the increased upward curvature of the jet in the bulk of the mould in the 3D results, clearly pointed out in Figure 4.9. The result is a higher impingement point on the narrow face of the mould with the 3D model (note that this is mostly on the centre plane).

According to Thomas (and agreed to by the author), this curvature in the 3D model is caused by the upward lifting force on the broadening 3D jet due to

the reduced pressure in the upper recirculating zone [2]. As Figure 4.9 illustrates, the 2D (flat) jet broadens less, consequently retaining more momentum (than the 3D jet) in order to resist this upward bending.

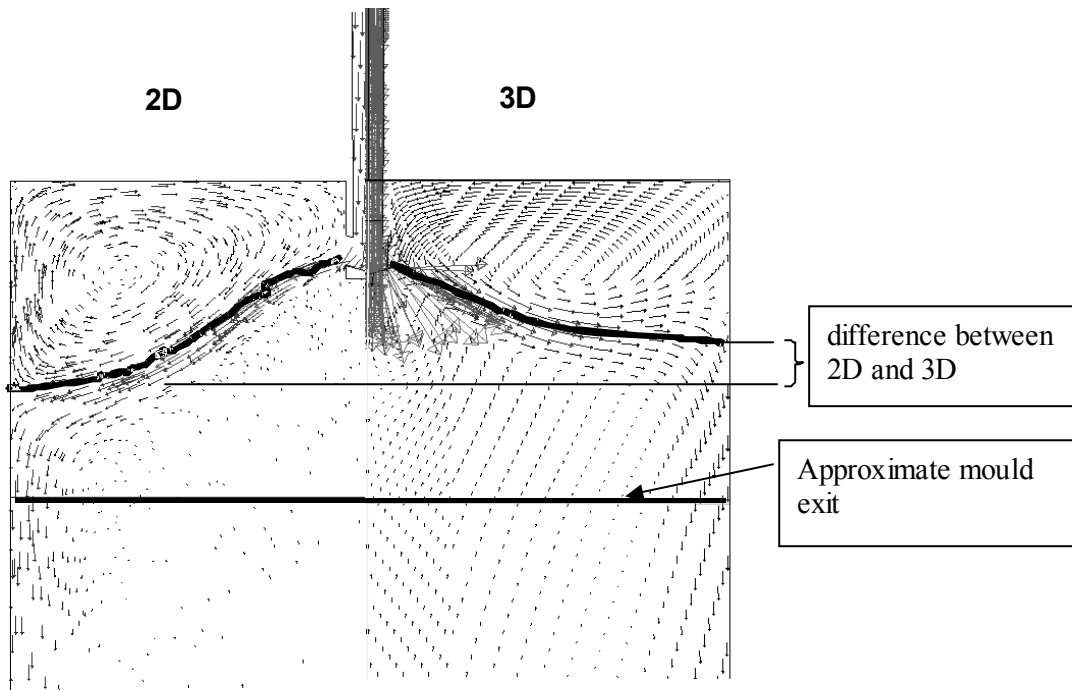


Figure 4.9: Comparison of 2D and 3D velocity predictions on centre plane of mould for 3D (base case SEN design)

Nevertheless, the true 3D nature of the jet flow will be illustrated in the following section, collaborating the above explanation.

#### 4.5 CFD model of steel plant

As depicted in the diagram in Figure 4.1, firstly the momentum CFD models were developed for CFD model verification.

The next step, now that the author is quite confident in the accuracy of the CFD modelling process, is to extend the model to be able to imitate the real steel plant circumstances.

All the preceding information in this chapter serves the purpose of a stepping-stone for the final 3D CFD model of the base case SEN design.

#### **4.5.1 Geometry and gridding strategy**

A 3D quarter model geometry and mesh were constructed using approximately 500 000 exclusive hexahedral cells. As described earlier in this chapter, a special function in GAMBIT [11] had to be employed to eliminate tetrahedral cells: a virtual geometry and accompanying virtual hex-mesh were created before exporting the mesh to FLUENT to set up all CFD parameters.

#### **4.5.2 Boundary conditions**

All the adiabatic walls (indicated in Figure 4.5) are replaced with walls with predetermined heat fluxes and temperatures, amongst others. The heat fluxes are estimated from 1D heat transfer simulations of the shell and mould. (Based on work of BG Thomas [2] and [52] ( $300\text{kW/m}^2$  becomes  $60\text{kW/m}$  for  $0.2\text{m}$  wide 2D case)).

The meniscus surface was modelled as a slip wall with a predetermined heat flux towards the surroundings. The walls of the mould cavity were modelled with downward moving walls (at casting speed of  $1.0\text{ m/min}$ ), while the walls were kept at the liquidus temperature ( $1450\text{ }^\circ\text{C}$ ) of the molten steel.

The mould cavity outlet was modelled as a pressure outlet at atmospheric pressure. Choosing this boundary condition far enough away from the SEN, the influence on the flow patterns surrounding the SEN will be small.

The inlet face at the top of the SEN was modelled as a velocity inlet, matching the mass flow rate of the steel corresponding to a casting speed of 1.0 m/min.

Owing to the assumption of full symmetry, the centre planes (wide and narrow) are defined as symmetry faces or boundaries.

### **4.5.3 CFD options and assumptions**

Firstly, full symmetry was assumed due to the fact that a quarter model mesh was used<sup>11</sup>, as already stated in section 4.5.2 above.

The flow was assumed to be steady-state. Although the author did encounter some SEN and mould cases (verified by water model test) where the jet seemed to be oscillating about an average position, most SEN designs demonstrated a steady jet angle and flow pattern.

Operating conditions were specified as being standard atmospheric pressure (101.3 kPa) and temperature of 20 °C. Gravity was switched on at 9.81 m/s<sup>2</sup>, which will of course have a buoyancy influence on the hotter emerging jet (albeit practically negligible [2]).

The turbulence model chosen for 3D CFD modelling is the k- $\omega$  turbulence model of Wilcox [10][50]. Although the RSM turbulence model is clearly the superior model for 3D due to its anisotropic evaluation of turbulence (as opposed to k- $\epsilon$  and k- $\omega$  -models' assumption of isotropic turbulence), it is far too expensive for optimising purposes. The Standard k- $\omega$  turbulence model is however “tweaked”<sup>12</sup>

---

<sup>11</sup> Refer to Chapter 6 where complete SEN and mould models are discussed for potential future work. Robustness and reliability studies should be performed on SEN design for the event that one port may be smaller than the other due to manufacturing tolerances, for example.

<sup>12</sup> Refer to section 4.3.3 for all the detail and comparisons between the turbulence models available in FLUENT.

to predict high shear flows and especially jet flow very accurately for 3D models as well.

The standard near-wall function was selected for this model (to predict flow accurately close to walls, by modelling turbulent boundary layers).

More complex phenomena like solidification and oscillating mould were not modelled.

#### **4.5.4 Solution procedure**

In essence, the same solution procedure was followed as described in section 4.3.4. However, due to the use of a virtual mesh, normal grid adaption (for mass imbalances and  $y^+$  adaption for near-wall functions) is not possible.

However, dynamic grid adaption is used instead, where the mesh is refined and/or coarsened as the solution proceeds (hence “dynamic”) based on velocity gradients (chosen for this case). This is an attempt to follow the formation of the SEN jet with grid clustering, and to keep the number of cells as low as possible.

#### **4.5.5 CFD Results and discussion**

Following the solution procedure, after approximately 30000 iterations, the solution was considered to be converged sufficiently.

The history of residuals (only the first 10000 are shown) in Figure 4.10 below shows the typical convergence history when dynamic grid adaption is employed. Each spike indicates when dynamic adaption occurred. Again, the switch to 2<sup>nd</sup>-order accuracy influenced the convergence stability, as the residuals seem to become unstable from that moment.

To ensure that the solution has truly converged, the maximum turbulent kinetic energy (TKE)<sup>13</sup> on the meniscus is displayed in Figure 4.11 as a function of each iteration. The convergence of a physical property of the CFD model towards a steady value, coinciding with sufficient and significant residual drops, constitutes a converged solution. The failure of the maximum meniscus TKE to reach a steady value (Figure 4.11) provides an indication of the possible unsteady nature of the solution. A time accurate transient simulation is required to verify this, although the water modelling experiments tend to indicate that the flow field is steady.

Admittedly, the residuals for the 3D CFD model of the base case (presented in Figure 4.10) suggest that the solution might not be converged. However, the following reasons might be blamed:

- The flow seems to be pseudo-transient, as also reflected by Figure 4.11. Pseudo-transient flow has been experienced to be more pronounced with wider mould widths, as the history of residuals is much more stable and convergent with narrower width moulds (3D exploration study in Chapter 5).
- The dynamic mesh adaption methods used (in an effort to control mesh sizes) seem to prohibit the residuals from stabilising. As soon as the solution starts to converge, the grid changes and the residuals are simultaneously enlarged. More work on dynamic adaption methods is necessary in future work.

The mesh quality is outstanding (100% hexahedral cells), and is thus not suspected as being the main culprit, although this possibility cannot be ruled out completely.

---

<sup>13</sup> In Chapter 5, this measurement will play a significant role in the objective function during the optimisation of the SEN.

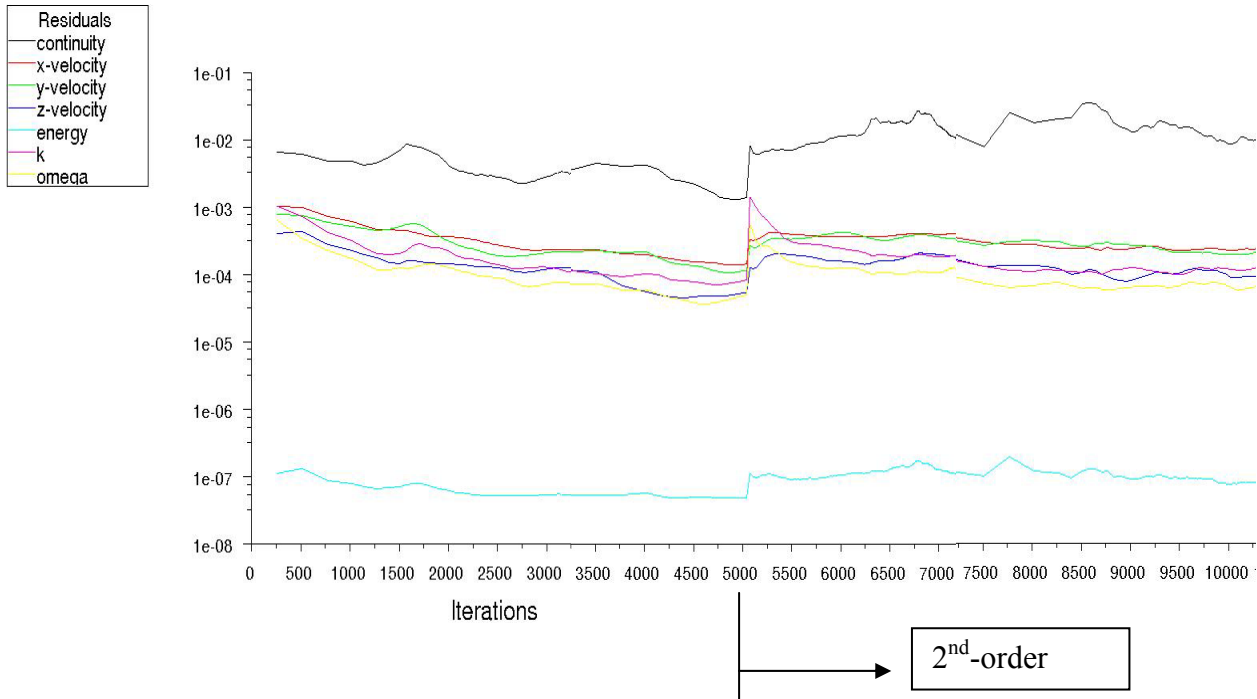


Figure 4.10: Residuals history (as a function of iteration number)

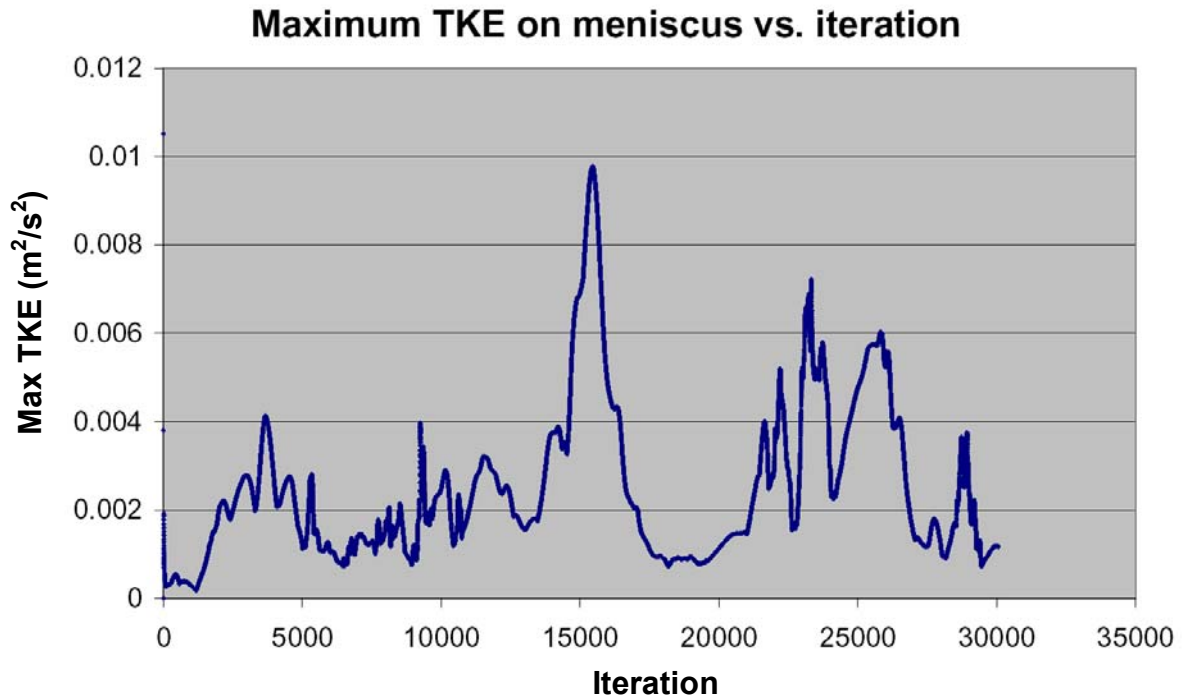


Figure 4.11: Physical property (maximum TKE on meniscus) as a function of iteration number

It is noticeable in Figure 4.11 that there is noise in the physical measured property (maximum TKE on meniscus in this case) as the solution progresses. If a certain

property were to be used as part of the objective function for optimisation purposes (Chapter 5), the specific property would need to be averaged in order to obtain a more representative value.

The results of the 3D CFD half model are displayed symmetrically in Figures 4.12 to 4.20, in the form of:

- contours of velocity and vorticity magnitude on the symmetry plane (*i.e.*, centre plane) (Figures 4.12 and 4.13)
- contours of helicity<sup>14</sup> on the symmetry plane (Figure 4.14)
- contours of turbulent kinetic energy (TKE) on symmetry plane (Figure 4.15)
- contours of shear stress on the wide mould walls (Figure 4.16)
- contours of temperature on the symmetry plane (Figure 4.17)
- path lines originating from the SEN inlet, coloured by vorticity magnitude (Figure 4.18)
- iso-surfaces of velocity magnitude coloured by turbulent kinetic energy (Figure 4.19), and
- velocity vectors scaled and coloured by its magnitude (Figure 4.20).

The turbulent kinetic energy on the meniscus surface (plan view) is displayed in Figure 21.

Different features of the jet and its three-dimensional shear layers can be discerned when comparing these results. E.g., path lines (Figure 4.18) and velocity vectors (Figure 4.20) illustrate recirculating behaviour, whereas vorticity magnitude (Figure 4.13) shows the extent of the jet shear layer. The impingement location (important to prevent breakouts if this location is below the mould exit) is most clearly depicted using path lines and helicity contours (Figure 4.14).

---

<sup>14</sup> Helicity identifies the core of streamwise longitudinal vortices. By definition, normalised helicity represents the cosine of the angle between velocity and the vorticity vectors. The sign of helicity is dependent on the orientation of the local velocity vector relative to the vorticity vector. Thus the core of a streamwise vortex can be identified as the region of high helicity. Boundary layers are regions of high vorticity and low helicity [10].



The turbulent kinetic energy contours (Figure 4.15) show that the kinetic energy is mostly concentrated inside the jet, as expected.

Figure 4.12, displaying contours of velocity magnitude on the centre plane of the 3D model, does not illustrate the true 3D nature of the flow, and the flow appears to be purely 2-dimensional.

However, the wall shear stress contours (Figure 4.16) clearly indicate the 3D nature of the flow that takes place inside the mould: the yellow areas on the mould wall indicate that the jet dissipates (and lifts) as it propagates along the wall towards the narrow mould wall. This corresponds to the initial water model experiments discussed in section 4.4.1.

The path lines (Figure 4.18) further illustrate the 3D flow patterns, as well as the complexity of the flow (secondary recirculating zones above jet exits). The iso-surface of velocity magnitude contour (Figure 4.19) confirms the strange jet behaviour highlighted by the path lines and shear stress walls figures: the “ends” of the jet lift up as the jet moves through the mould towards the narrow wall. It is evident from this figure that the jet centre line (on the centre plane of the mould) is lower than the sides or ends of the jet.

Figure 4.17, displaying contours of temperature magnitude on the centre plane, clearly shows that the boundary condition on the mould walls is satisfied, where the mould walls are at the lowest temperature (in the accompanying temperature scale), corresponding to the steel liquidus temperature (1723 K or 1450 °C). As expected, the (high) temperature of the jet is rapidly dissipated into the mould cavity. The double recirculation zones (upper and lower) are also easily spotted in this figure.

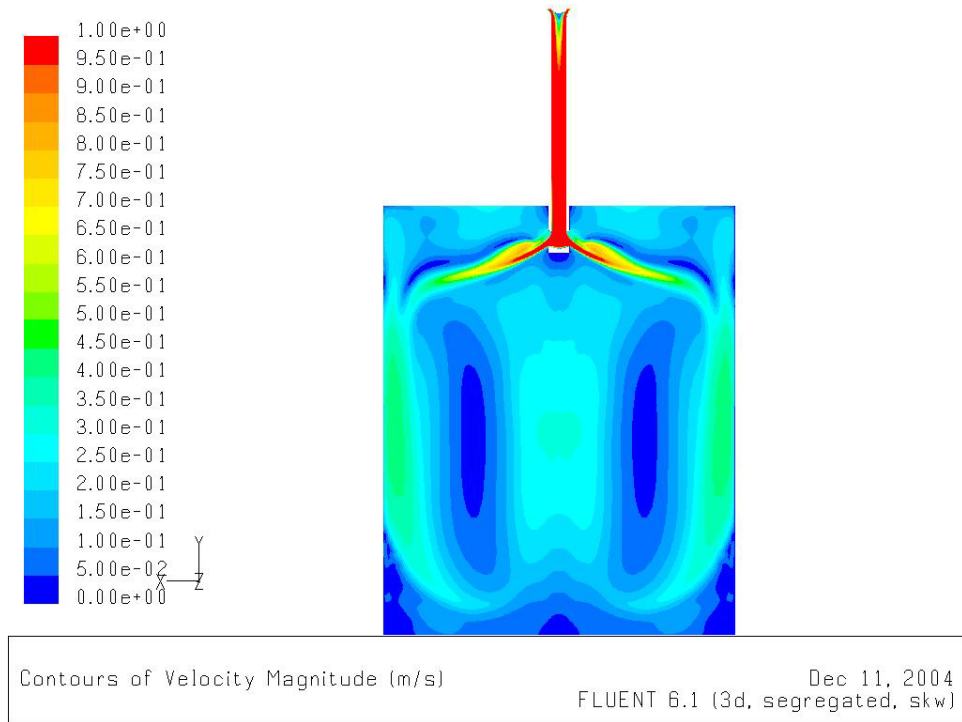


Figure 4.12: Base case velocity magnitude contours on symmetry plane: range 0 – 1 m/s

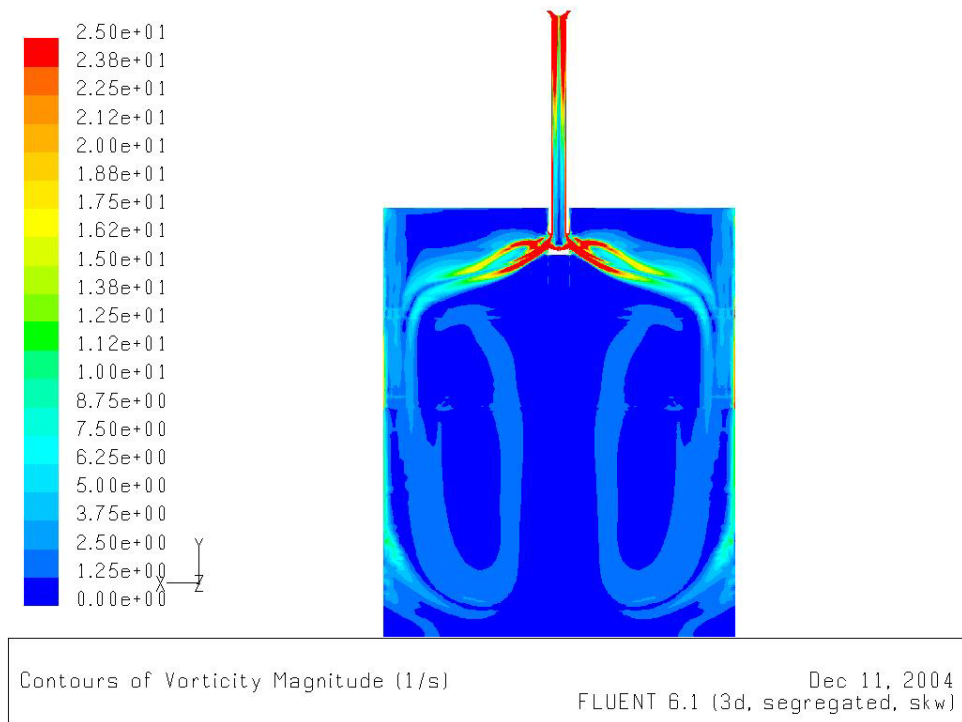


Figure 4.13: Base case vorticity magnitude contours on symmetry plane: range 0 – 25 1/s

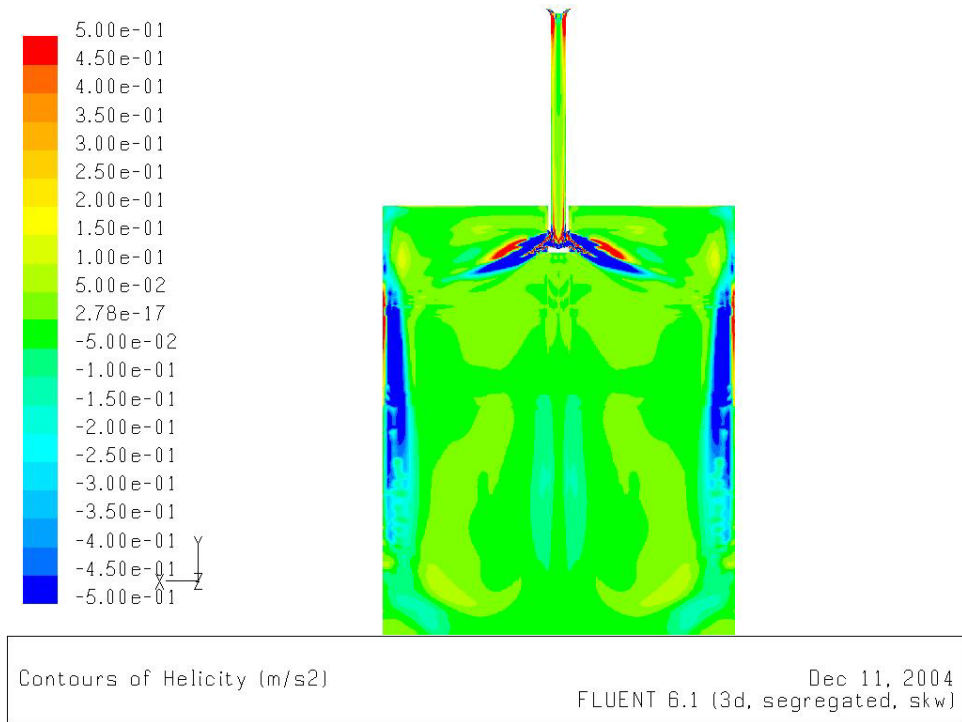


Figure 4.14: Base case helicity magnitude contours on symmetry plane: range -0.5 – 0.5 m/s<sup>2</sup>

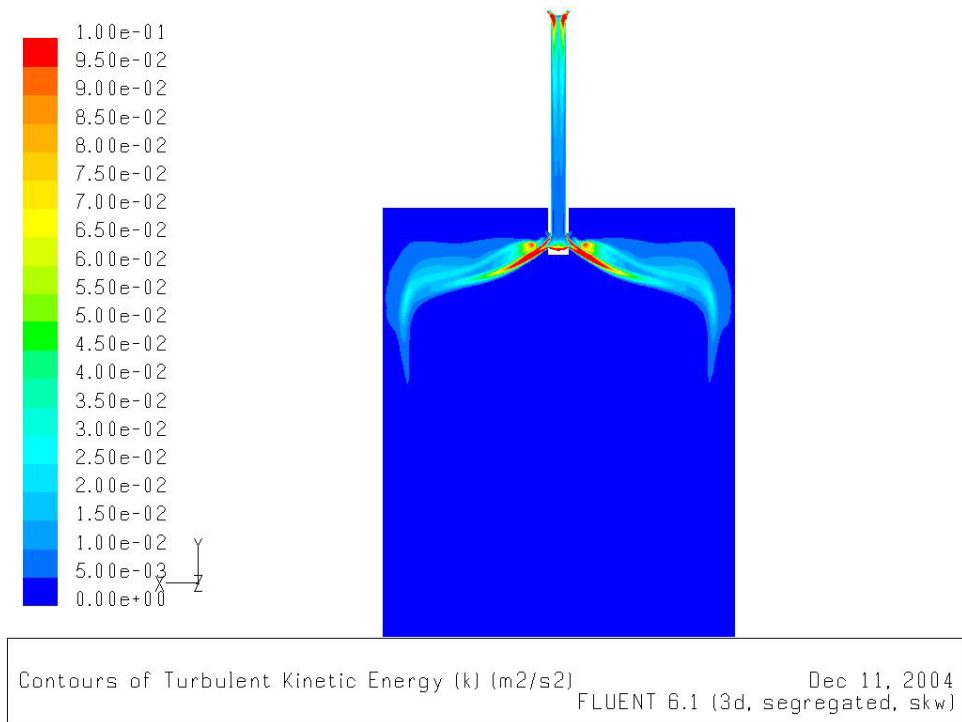


Figure 4.15: Base case turbulent kinetic energy contours on symmetry plane: range 0 – 0.1 m<sup>2</sup>/s<sup>2</sup>

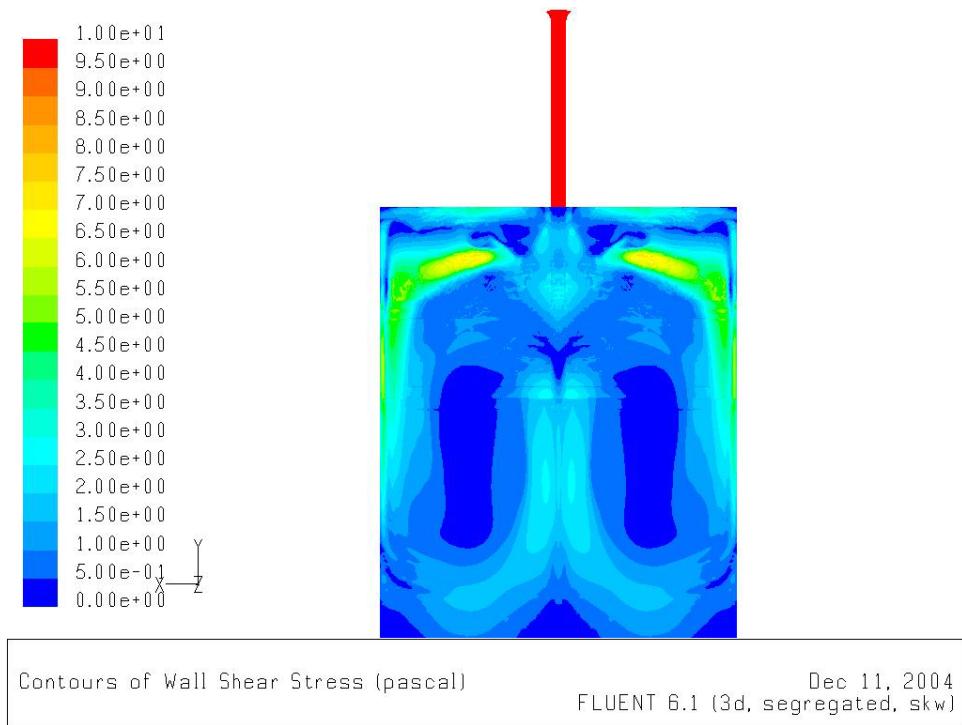


Figure 4.16: Base case wall shear stress contours on wide mould face: range 0 – 10 Pa

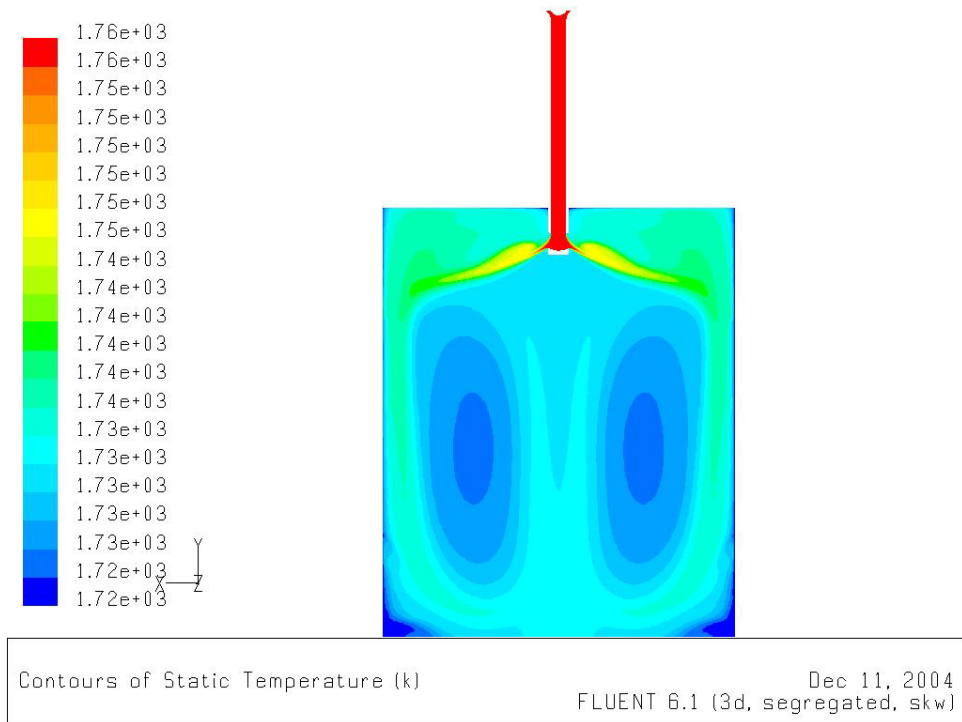


Figure 4.17: Base case temperature contours on symmetry plane: range 1723 – 1758 K

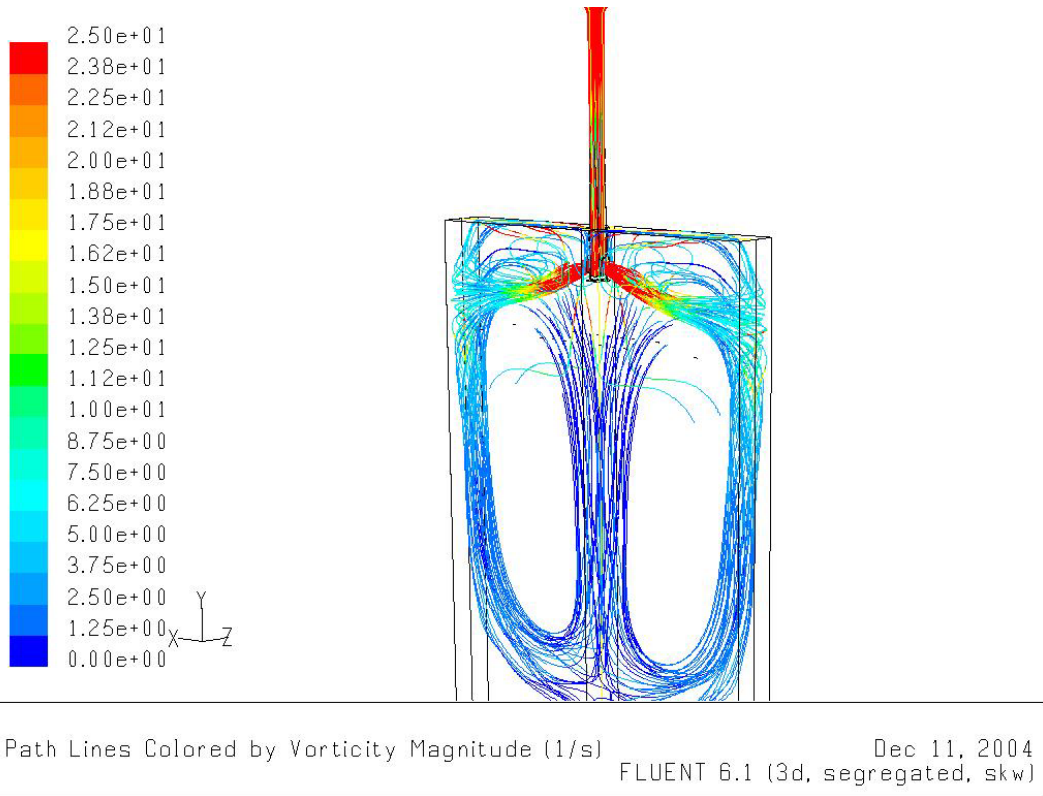


Figure 4.18: Base case path lines coloured by vorticity magnitude: range 0 – 25 1/s (isometric view)

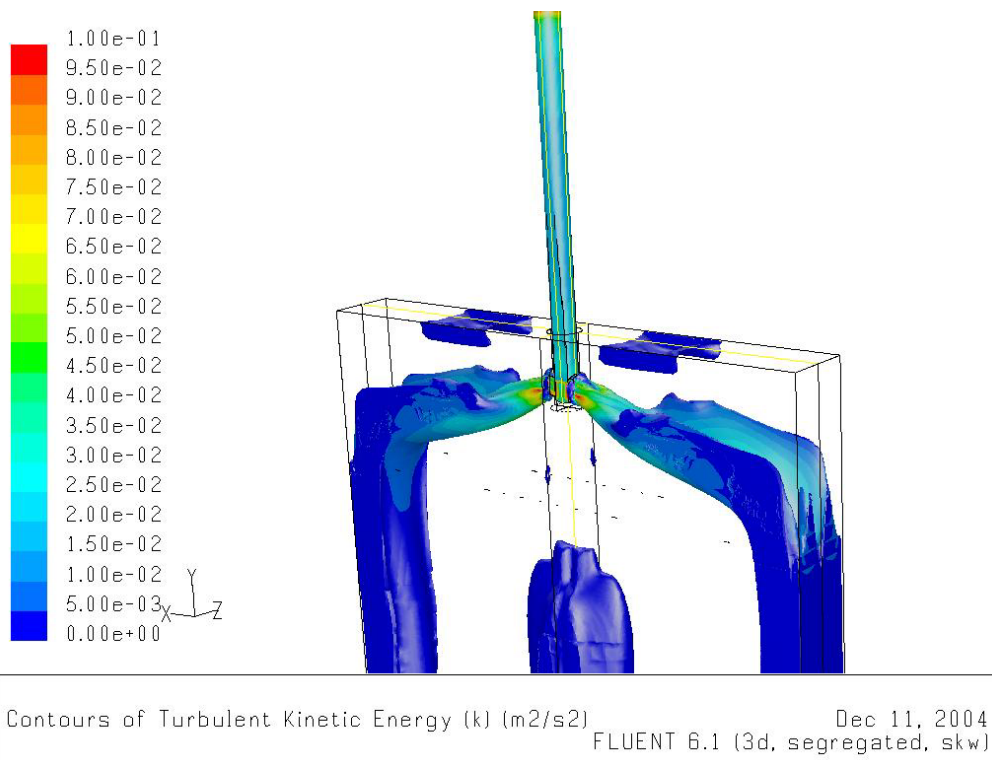


Figure 4.19: Base case iso-surface of velocity magnitude ( $v=0.25\text{m/s}$ ) coloured by turbulent kinetic energy: range 0 –  $0.1\text{ m}^2/\text{s}^2$

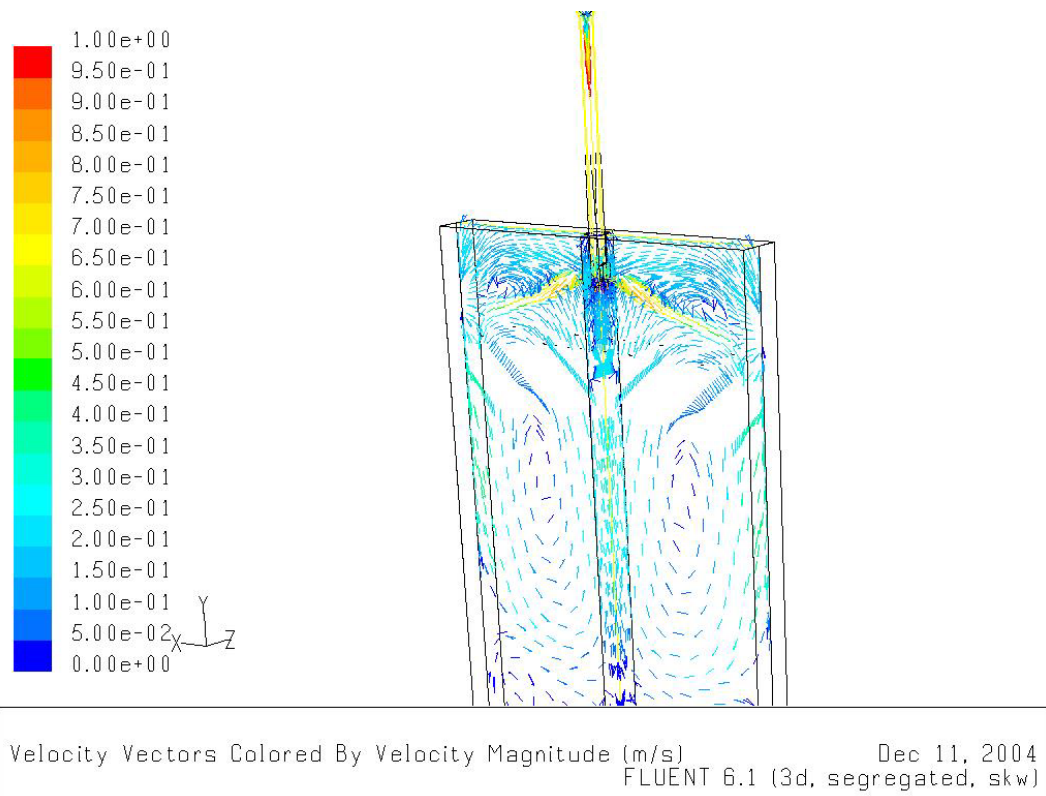


Figure 4.20: Base case velocity vectors coloured by velocity magnitude: range 0 – 1 m/s (isometric view)

The turbulent kinetic energy on the meniscus surface is shown in Figure 4.21, illustrating the approximate positions where the maximum TKE occurs on the meniscus. The figure is of a specific iteration and changes with each iteration (refer to Figure 4.11), and appears to be transient in nature. In Chapter 5, the maximum TKE on the meniscus surface will play a significant role in the optimisation process of the SEN and mould.

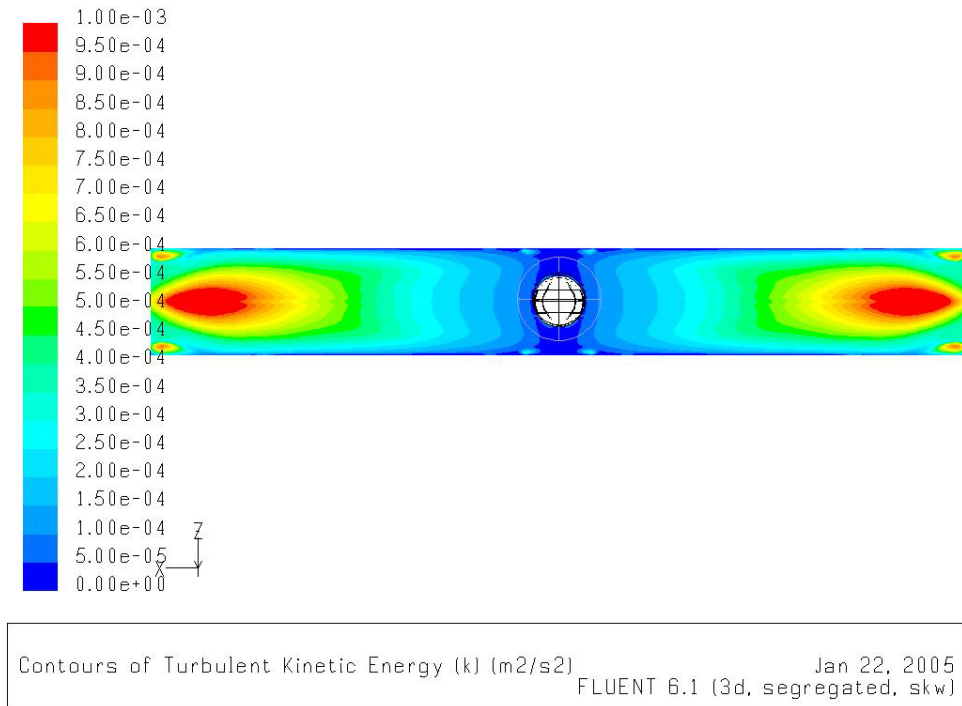


Figure 4.21: Base case turbulent kinetic energy contours on meniscus surface: range 0 – 0.001 m<sup>2</sup>/s<sup>2</sup> (top view)

#### 4.6 CFD SEN and mould model: reduced widths

The initial base case and starting point of this study involved the 1575mm width slabs, as Columbus Stainless (a major initiator of the study topic) experienced the most quality problems on this width (their maximum width). As mentioned earlier in this chapter, a number of problems regarding the CFD modelling resulted in so-called unphysical flow solutions. Some inconsistencies still exist with models of the widest width.

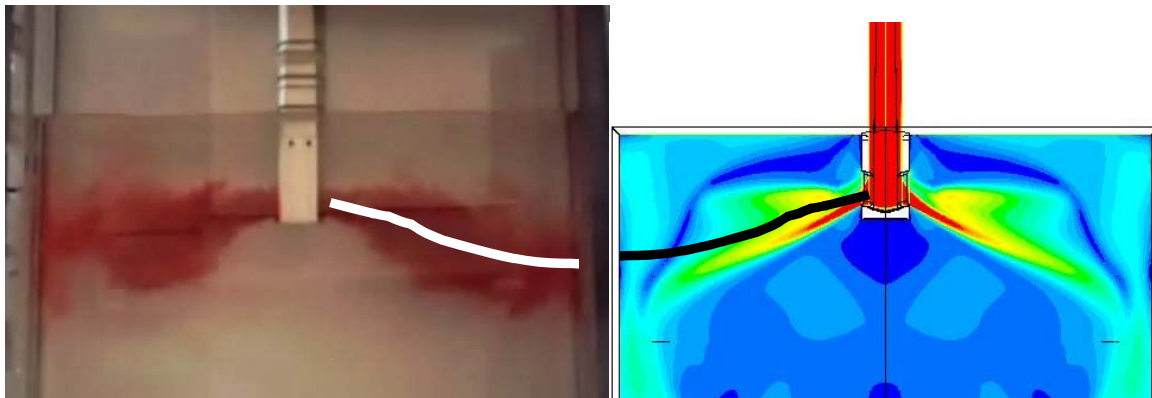
However, recently Columbus Stainless requested an optimum SEN design specifically for narrower slab widths (range 1000mm – 1300mm)<sup>15</sup>. Naturally, CFD models of these narrower widths were carried out, with surprising results:

<sup>15</sup> Owing to availability of ADVENT full-scale water model results (also verified with UP 40%-scaled water model results), the widths 1060mm and 1250mm were chosen as representative for the 1000 – 1300mm range.

The 1060mm and 1250mm width results corresponded closely to water model validation (full-scale and 40%-scaled) results.

Refer to Figure 4.22 showing the good correspondence between the 3D CFD model velocity magnitude contours with the 40% water model test.

1060mm width; 80mm submergence depth; 1.1m/min casting



UP 40% water model

CFD  $k-\omega$  turb model

Figure 4.22: Comparison: Old SEN 40%-scaled water model with 3D CFD model (contours of velocity) on centre plane

An interesting observation was that the submergence depth does not have a major influence on the jet angle – it is mostly determined by the SEN design (port height, angle, amongst others). Figure 4.23 clearly illustrates this point: the CFD model at a (full-scale) submergence of 80mm, visualised using path lines, corresponds accurately to the jet pattern of the 40%-scaled water model, at a much deeper submergence depth of 150mm (full-scale). The SEN design used in Figure 4.23 is the base case (old SEN) as described in section 4.2 of this chapter.



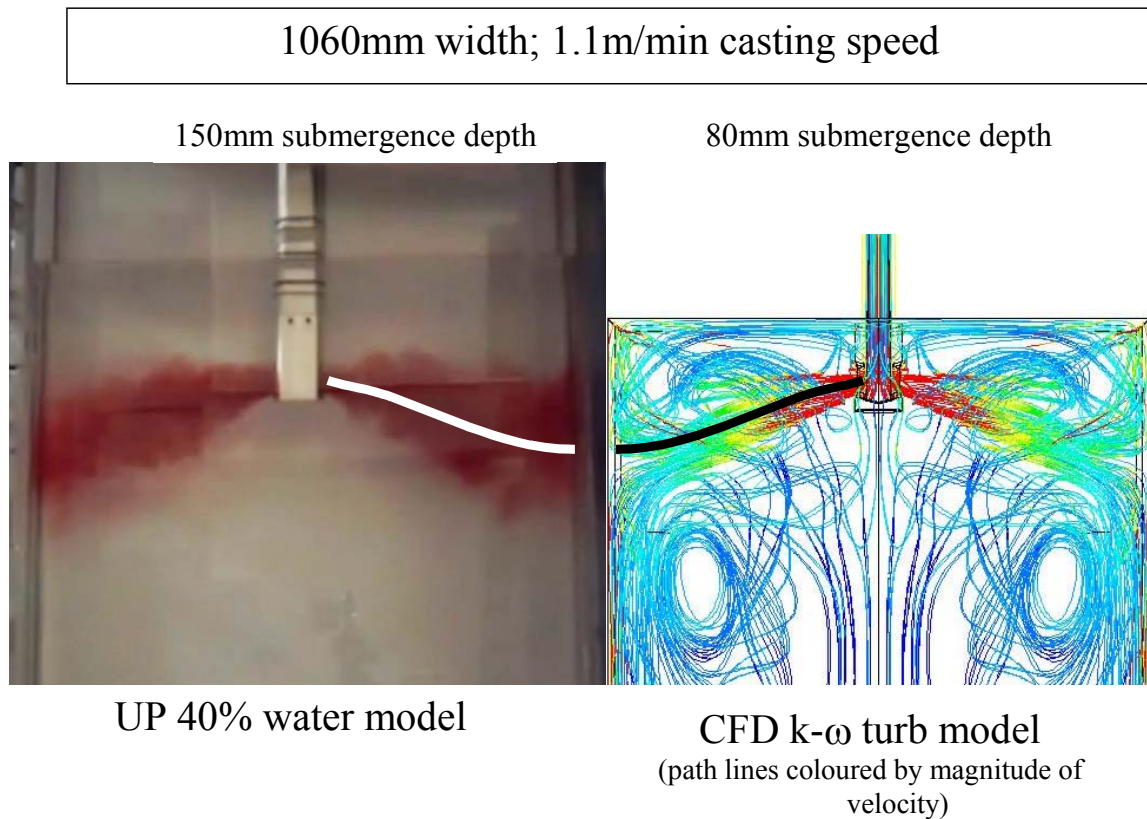


Figure 4.23: Submergence depth does not influence jet angle significantly at Fr-similarity flow rate

The improved correspondence of the CFD models of the narrower widths with water modelling can be attributed to the more stable solution procedure (as opposed to the somewhat erratic residuals history of the 1575mm wide CFD models). Not only are more cells necessary for the wide widths, but also the effect of the isotropic turbulence assumption model seems to influence the jet characteristics in the larger mould cavity. Usually, the jet seems to rise or “pick up” as it nears the mould wall, presumably as it runs out of momentum due to the spread-out of the jet in the mould cavity. The author believes that this can be partly attributed to the (incorrect) assumption of isotropic turbulence.

In Chapter 6, some suggestions are made with respect to CFD options to eliminate the deviations from the real (water modelled) flow, especially for the widest and coincidentally the most problematic widths.

#### **4.7 Conclusion of base case CFD modelling**

This chapter has illustrated CFD modelling of the SEN and mould base case as the stepping-stone towards SEN optimisation with CFD.

A typical approach to any CFD simulation problem was illustrated using a diagram. This approach was applied to the base case for this dissertation, which is the SEN currently used by Columbus Stainless, Middelburg, South Africa:

Firstly, the base case was described in detail and certain assumptions were motivated (e.g., simultaneous SEN and mould modelling, 2D vs. 3D modelling, etc.). Thereafter, the CFD set-up was described, including choice of mesh elements, boundary condition assumptions, choice of turbulence model, the solution procedure, to name but a few. A momentum-only model was created to mimic water model conditions for initial water model validation purposes.

After being confident that the CFD modelling of the water model was accurate, the next step was to extend the CFD model to be able to imitate the real steel plant circumstances. The solution of the full-scale CFD model of the real plant base case was illustrated using a number of visualisation techniques. The (possible) transient nature of the flow was also highlighted, which should be taken into account for optimisation purposes (by averaging the properties that will be used for the objective function/s). Furthermore, it was shown that reduced mould widths resulted in a more stable flow field (of the CFD solution), which also confirms the fact that Columbus Stainless experiences the most quality problems with their largest slabs with a width of 1575mm.

In conclusion: the CFD modelling approach (including CFD set-up and solution procedure) to typical SEN and mould applications was perfected and optimised for the base case and other similar cases. These methods were verified by validating the CFD solutions with water model experiments. Optimisation using these CFD modelling techniques follows in the next chapter.